# GEOSTATISTICAL EVALUATION OF WELL LOGS IN RESERVOIR CHARACTERIZATION IN AZERI-CHIRAG-GUNESHLI FIELD

A THESIS SUBMITTED TO
THE GRADUATE SCHOOL OF NATURAL AND APPLIED SCIENCES
OF MIDDLE EAST TECHNICAL UNIVERSITY

BY

RAHIM RZAZADE

IN PARTIAL FULFILLMENT OF THE REQUIREMENTS
FOR
THE DEGREE OF MASTER OF SCIENCE
IN
GEOLOGICAL ENGINEERING

JUNE 2013

Approval of thesis:

GEOSTATISTICAL EVALUATION OF WELL LOGS IN RESERVOIR CHARACTERIZATION AND FLOW UNIT DETERMINATION IN AZERI-CHIRAG-GUNESHLI FIELD

submitted by **RAHIM RZAZADE** in partial fulfillment of the requirements for the degree of **Master of Science in Geological Engineering Department, Middle East Technical University** by,

Prof. Dr.Canan Özgen Director
Dean, Graduate School of **Natural and Applied Sciences** _____

Prof. Dr. Erdin Bozkurt
Head of Department, **Geological Engineering** _____

Prof. Dr. Nurkan Karahanoğlu
Supervisor, **Geological Engineering Dep., METU** _____

**Examining Committee Members**

Prof.Dr. Serhat Akın
Petroleum and Natural Gas Engineering, METU _____

Prof.Dr. Nurkan Karahanoğlu
Geological Engineering, METU _____

Prof.Dr. Tamer Topal
Geological Engineering, METU _____

Assoc. Prof. Dr. İsmail Ömer Yılmaz
Geological Engineering, METU _____

Y.Müh. Tacettin Dölek
TPAO _____

**Date:** _____

**I hereby declare that all information in this document has been obtained and presented in accordance with academic rules and ethical conduct. I also declare that, as required by these rules and conduct, I have fully cited and referenced all material and results that are not original to this work.**

Name, Last name: Rahim Rzazade
Signature:

# ABSTRACT

## GEOSTATISTICAL EVALUATION OF WELL LOGS IN RESERVOIR CHARACHTERIZATION IN AZERI-CHIRAG-GUNESHLI FIELD

Rahim Rzazade
M.Sc, Department of Geological Engineering
Supervisor : Prof.Dr. Nurkan Karahanoğlu
June 2013, 85 pages

The Azeri-Chirag-Guneshli (ACG) field is situated offshore of Caspian Sea Azerbaijan sector. It is an elongated anticline in structure and the reservoir section consists of mainly sandstone. Recoverable reserves are calculated to be 5.4 bbl of oil (Binyatov 2008). Sedimentary environment corresponding to this region is mainly fluvio-deltaic.

The main aim of this study is to obtain better understanding of two main prolific hydrocarbon reservoir Pereriv B and Pereriv D by integration of well logs and core data. Moreover, flow unit determination was also very important point of this study. The work represents a petrophysical-based method that uses well loggings and core plug data to delineate flow units within the most productive sandstone reservoir in Azeri-Chirag-Guneshli field.

Nine wells are avaliable for this work and 6 of them have core data.Geostatistical methods such as histogram analsis and principal component analysis have been used for each formation. Based on well log data petrophysical parameters such as porosity, volume of shale, saturations have been estimated and they are integrated with core plug data. From the well logs it was obtained that the both Pereriv B and Pereriv D formations have high NTG ratio.Moreover, one flow unit have been determined within a Pereriv B formation based on core data such as porosity, permeability and proe throart size. These parameters was observed to be high in flow unit. Moreover, histogram and Principal Component Analysis showed that Pereriv B and Pereriv D formations are similar to each other. Although the statistical methods could not find any new flow unit but the studies gave a good result in comparision of two different formations.

Key words: Azeri-Chirag-Guneshli field, Caspian Sea, Azerbaijan, Pereriv B, Pereriv D, flow unit, well logs, geostatistics, histogram analysis, principal component analysis

# ÖZ

## AZERİ-ÇIRAQ-GÜNEŞLİ SAHASININ REZERVUAR KARAKTERİZASYONUNDA KUYU LOGLARININ JEOSTATİSTİKSEL DEĞERLENDİRMESİ

Rahim Rzazade
Yüksek Lisans, Jeoloji Mühendisliği Bölümü
Tez Yöneticisi: Prof.Dr. Nurkan Karahanoğlu
Haziran 2013, 85 sayfa

Azeri-Çıraq-Güneşli sahası Hazar Denizi`nin Azerbaycan kısmında yerleşmektedir. ACG, antiklinal yapıya sahip olup rezervuar kısmı ağırlıklı olarak kumtaşından oluşmuştur. Rezervlerin 5.4 milyar varilinin çıkarılabileceği hesaplanmıştır. Bu bölgedeki çökelme ortamı daha çok flüvyal deltaya karşılık gelmektedir.

Bu çalışmanın asıl amacı, iki ana verimli hidrokarbon rezervi olan Pereriv B ve Pereriv D`yi kuyu logları ve karot bilgilerini kullanarak daha iyi anlamaktır. Ayrıca, akış ünitelerinin saptanması bu çalışmada önemli bir yere sahiptir. Bu çalışma, sahanın en verimli kum taşı rezervi olan Pereriv B`nin formasyonlarının akış birimlerinin taslağını çizmek için kuyu loglarını ve karot bilgilerini kullanan petrofiziksel bir yöntemi temsil etmektedir.

Bu çalışmada kullanılabilecek 9 kuyu vardır ve bunların 6 tanesinin karot bilgisi vardır. Herbir formasyon için histogram analizi ve temel bileşen analizi gibi jeoistatistiksel yöntemler kullanılmıştır. Kuyu loglarının verilerine dayanarak gözenek, kil hacmi, doyumluluk gibi petrofiziksel parametreler tahmin edilmiş ve bunlar karot verileriyle bütünlenmiştir. Pereriv B ve Pereviv D`nin yüksek kumluluk oranlarına sahip olduğu kuyu loglarından çıkarılmıştır. Ayrıca, Pereriv B`nin bünyesinde gözenek, akışkanlık ve gözenek boyutu gibi karot bilgilerine dayanan bir akış birimi belirlenmiştir. Bu parametreler akış birimlerinde yüksek değerler almaktadır. Üstelik, histogram ve temel bileşen analizi, Pereriv B ve Pereriv D`nin formasyonlarının birbirlerine benzediklerini göstermiştir. İstatistiksel metodlar Pereriv D`de akış birimi bulmada çok fazla faydalı olmamalarına rağmen iki farklı formasyonun karlılaştırılmasında iyi sonuç vermişlerdir.

Anahtar kelimeler: Azeri-Çıraq-Güneşli sahası, Hazar denizi, Azerbaycan, Pereriv B, Pereriv D, akış birimi, kuyu logları, jeostatistik, histogram tahlili.

To my family

## ACKNOWLEDGMENTS

I would like to express my deepest gratitude to my supervisor, Prof.Dr. Nurkan Karahanoğlu, whose expertise, understanding, encouragement and patience, added considerably to my graduate experience. I appreciate his vast knowledge and skill in many areas, and his assistance in writing this thesis.

I would like to express my grateful appreciation to my family for their support and encouragements all the way through my study at METU.

I would like to express my gratitude to BP Caspian Sea Exploration for providing me with scholarship and financial support. Thanks to Azerbaijan State Oil Company and BP Caspian Sea Exploration for giving me permission to work on data from Caspian Sea.

# TABLE OF CONTENTS



**CHAPTERS**

# LIST OF TABLES

## TABLES

# LIST OF FIGURES

## FIGURES

# CHAPTER 1

# INTRODUCTION

Reservoir characterization is one of the key processes to obtain better understanding of the flow ability and storage capacity of petroleum reservoir. Usually sandstone reservoirs make challenges for petroleum engineers and geoscientist to obtain reliable information about it because of their ability to be cemented and heterogeneous due to post depositional and diagenetic alterations. One of the uncertainties found in clastic reservoirs can be shown by the large variability seen mostly in porosity/permeability crossplots gained from conventional core data analysis.

Characterization of sandstone reservoirs such as subdividing it into flow units is a special way of reservoir zonation. Particular petrophysical elements such as pore throat radius, permeability, porosity, water saturation, storage and flow capacity can be very useful in determination of the presence of distinct units which help researchers to make reliable reservoir characterization. The biggest advantage from determination of the flow units can be got in the early life of the reservoir because it gives better prediction of the future reservoir performance.

A hydraulic flow unit (HFU)is determined as the indication volume of total reservoir rock within which physical and geological factors that cause fluid flow are internally consistent and understandably different from features of other rocks (Ebanks et all., 1984). A hydraulic flow unit is a zone of the reservoir which is continuous both horizontally and vertically exhibit similar flow characteristics.

Understanding of permeability is a crucial step in establishing a reliable reservoir description. Reservoir permeability highly affects the strategies of the well completions and stimulation and reservoir management. There are some methods to identify reservoir permeability such as well testing, coring, and conventional well loggings. Due to high cost of coring, usually limited number of wells can be cored. However, some alternative ways can be used in determination of the permeability. The most applicable one is to estimate the permeability from well logs. The reason is that logging does not cost as much as coring. A disadvantage of well log derivation of permeability is heterogeneity of the sandstone reservoir that makes a difficulty and problems. A basic correlation between permeability and porosity can not be established, due to the effect of other well log parameters that are needed to be embedded into the correlation. Besides all of these challenges for permeability estimation from well logs, using wireline log data provides a continuous permeability profile throughout the particular interval that can be described as a hydraulic flow unit (Al-Ajmi et al, 2000).

The Azeri Cirag Guneshli Oil Field is located to the South East of Baku, offshore Azerbaijan (Figure 1) in water depths ranging 60m-280m (Binyatov 2008). The field structure consists of three connected culminations, which are, from west to east Shallow Water Guneshli, Deep Water Guneshli, Chirag and Azeri. The ACG complex comprises approximately 135 square kilometers and the fields have been calculated recoverable reserves of about 5 to 6 billion barrels of hydrocarbon. Moreover, there are two main productive sandstone reservoir horizon called Pereriv B, and Pereriv D.


**Figure 1.** Location map of Azeri-Chirag Guneshli field

The filed has been operated by the consortium called Azerbaijan International Oil Company since 1994. The consortium is leaded by BP with 37.4% share. Also there are other international oil companies within the consortium such as TPAO 6.75%, Chevron 11.3%, SOCAR and Inpex 10%, StatoilHydro 8.5%, Itochu 3.9%, Hess 2.72%.

The aim of this study is to describe and characterize Azeri-Chirag-Guneshli filed by using core data and well log data from the wells drilled in the area. The distribution of reservoir properties concerning the petrophysical parameters are taken into account for a true hydraulic flow zonation. The well logs are analyzed for all available wells, and then the outcome is compared with core data information to obtain reliable estimates between parameters. All data obtained from cores and well logs are analyzed to model a petrophysically based flow units for ACG field with geostatistical methods.

## 1.1. Statement of Purpose

In Azeri-Chirag-Guneshli field 9 wells are available for this study. All of these wells penetrate to Pereriv B which consists of sandstone and shale alteration. Among those 9 wells only 7 wells are available in Pereriv D formation. Moreover, all wells have well logs and only 5 of them have core data. It is worthy to highlight that cores are taken only from Pereriv B

The main purpose of this work is to identify the flow units in Pereriv B, which is the most oil productive sandstone reservoir in ACG Field. The flow unit zonation concept is primarily based on the available core plug data measurements and the conventional well logging data. The basic geologic framework of the studied wells should be constructed by well log attributes. The study is followed by the core data analysis for the determination of the petrophysical framework. The core plug analysis is fitted within the methods and classifications available in the literature. A profile of various units can be obtained after the combination of this work. To reach the goal, geostatistical approaches are used for discrimination of similar data and groups. However, not all the available wells in the field are cored, for the continuity of defined unit delineation, wells with no cores will be chosen and permeability estimation will be tried to be applied within the geostatistical methods.

# CHAPTER 2

# LITERATURE SURVEY

## 2.1. SouthCaspianBasin

The area of interest is located in South Caspian Basin, Azerbaijan sector of offshore Caspian Sea where many researches about stratigraphical, sedimentological, lithological and petrographical properties of the reservoir units including the productive series of ACG filed are present.

Kevin et al. (2007) stated first detailed assessment of the role of big and intermediate scale heterogeneities on fluid flow. In this research experimental approaches have been performed to obtain the influence of different heterogeneities. An important achievement from this work was that connection between close high and low NTG reservoir units highly improves recovery, allowing pressure contribution and a route for oil migration from sand bodies within the poor NTG parts which would otherwise be isolated.

Francesco et al. (2001) worked on a project which was a case history of the characterization of a structure in the sector of Azerbaijan gained by application of seismic tools such as "3D Pre-Stack Depth Migration and Continuity Depth Cube volumes". This work was concentrated on the "Kurdash Permit" and close location of Azerbaijan of south most the country, close to Iran's boarder, situated in the west part of the South Caspian. It considers the techniques applied to illustrate the subsurface, the resultant model and implications for its geological history made visible by the advanced seismic tools.

Moreover, Reynolds et al. (2006) made researches on ACG field. And the paper was about variations in pressure that's seen with depth, location, stratigraphy and time are crucial to identify flow units and compartments in hydrocarbon reservoirs.

## 2.2. Hydraulic flow unit concept

Numerous methods were suggested to subdivide reservoir rocks into layers (these layers are mentioned as lithofacies, petrofacies, electrofacies, and hydraulic flow units or also called flow units).

Lucia et al. (1992) determined flow units carbonate-ramp reservoirs. The work was concentrated on finding mean number of petrophysical parameters within geological constraints and made an attempt to illustrate the 3D spatial distribution of petrophysical parameters in the formation.

Abbaszadeh, et al. (1995) also worked on prediction of permeability by hydraulic flow units applying Amaefule's method. First he calculated pore-throat related parameters of flow

zone indicator and reservoir quality index by using core information after it, they used cluster analysis for finding the probable hydraulic flow zones. The approaches include probability plot, Ward's analytical algorithm, and the histogram analysis. These methods give visual description of flow zone indicator distribution to identify the probable number of fs. Together analytical clustering methods with graphical methods can give a reliable result for dividing of hydraulic flow units.

Klimentos et al. (1995) joined seismic wave technology and petrophysics for making a new approach in reservoir characterizations and explorations of reservoirs in a hydraulic flow unit point of view

Gunter et al.(1997) highlighted the significance of finding of flow zones in a beginning of the field life, because such kind of an prediction will help a lot to obtain better information to detect flow units.

Ratchkovski et al. (1999) applied conventional methods and statistics for defining hydraulic flow units for better reservoir characterization. The variogram modeling petrophysical parameters have been constructed.

Lee and Datta-Gupta (1999) made a research on electrofacies characterization by the help of non-parametric regression techniques and multivariate analysis. In order to determine electrofacies and their classification, they utilized PCA, discriminant analysis, and model-based cluster analysis. In order to estimate permeability from well logs non parametric regression were performed. By using alternating conditional expectations (ACE) and neural networks (NNET) regression models were analyzed.

Porras et al. (1999) established a correlation among different flow units model. These zonations are different where hydraulic flow unit is recognized as a consistent with identical and average properties which have an influence on flow, petrofacies are characterized as zones with identical features

Rincones et al. (2000) made a study about flow unit context to determine an effective petrophysical fracture characterization. They utilized permeability-porosity relationship, reservoir quality index concepts, and flow zone indicator to deliniate flow units.

Aguilera etal. (2001) introduced different methodology for flow unit determination. They used Pickett crossplots of effective porosity versus true resistivity in order to obtain reservoir process speed, which is equal to k/Ø. Capillary pressure data, pore-throat apertures and Winland R35 values analysis are also included in their study to define hydraulic flow units.

# CHAPTER 3

# GEOLOGICAL BACKGROUND

## 3.1 Regional geological settings

The Caspian Basin is widely regarded as a remaining back arc basin of the Tethys Sea that evolved adjacent to the rapidly uplifting Greater Caucasus Mountains after the Paleogene Era (Zonenshain and Le Pichon 1986). One of the major processes which have been evolved in the formation of South Caspian basin's present shape and petroleum system were due to interaction between Indian, Arabian and Eurasian plates and numerous microplates (Figure2) (Golonka et al., 2002). The Caspian Sea and Black Sea were a part back-arc basin of Mesozoic chain stretching more than 3000 km. This also included the CarpathianBasin in central Europe and the Vallesian Trough in Switzerland (Dercourt et al., 1986). Neo-Tethys was south of the island-arc system. Zonenshain et al. (1986) mention that the basins formed after three different tectonic scenarios—in Mid and Late Jurassic, and Late Cretaceous times.

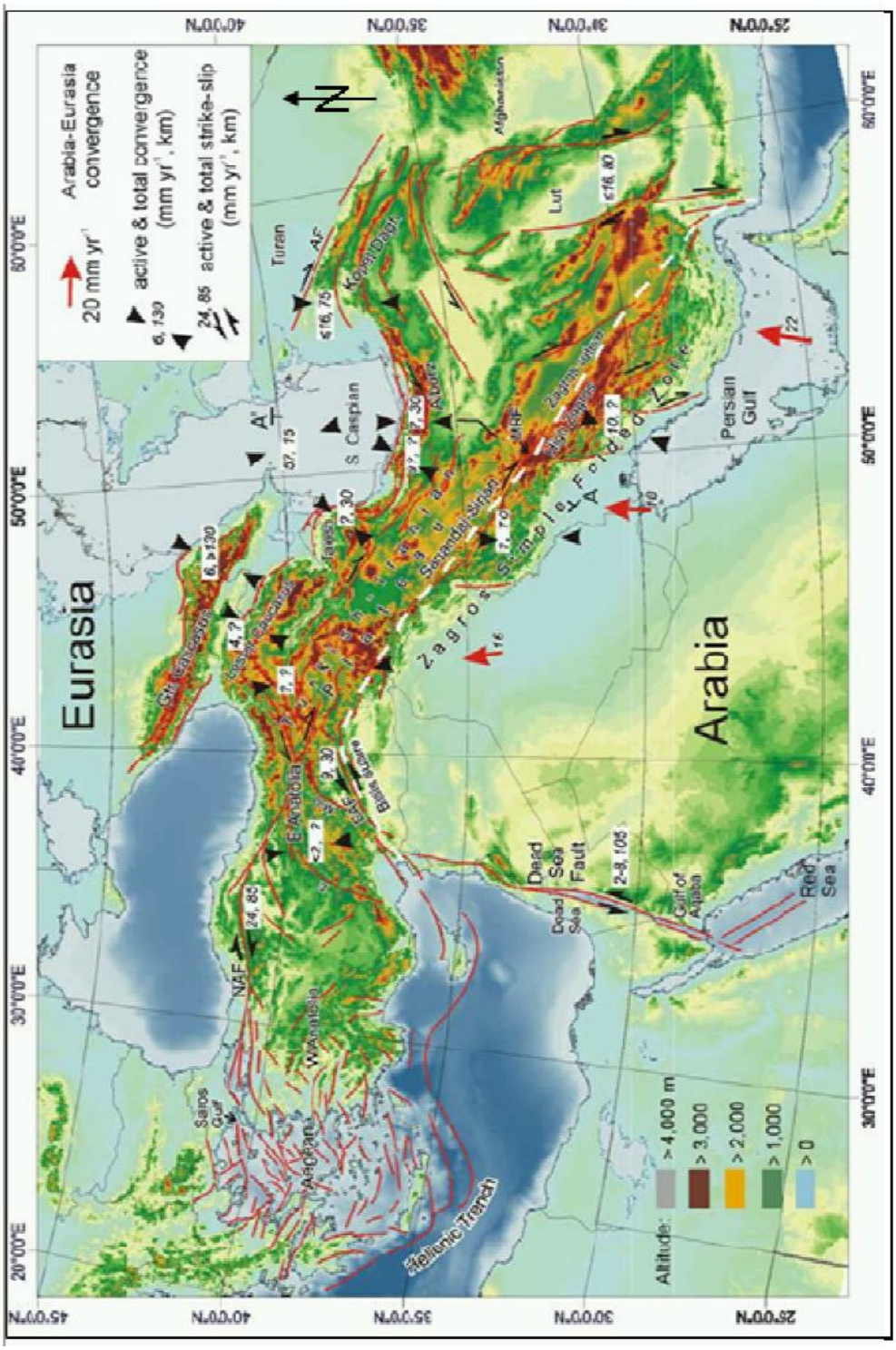


**Figure 2. .** Arabia – Eurasia Collisions. (adapted from Allen et. al., 2002)

From Middle Jurassic to Early Cretaceous time, extension occurred north of the Pontic-Trans-Caucasus arc, resulting in rifting and the formation of the early Black Sea and South part of the Caspian Basin. Toward the east, rate of spread was more rapid. This produced an oceanic basin, the remnants of which now form the South Caspian Basin. (Zonenshain et al., 1986).

Renewed interaction between the Eurasian and Arabian plates during Oligocene-Late Pliocene period started the separation of the Caspian Sea and the Black Sea. This process resulted in uplift of the Caucasus mountains, during the northward migration of the Iranian plate, the Elburz Mountains rose, causing separation of central Iran from the Caspian paleobasin (Smith-Rouchet et al., 2006) (Figure 3).

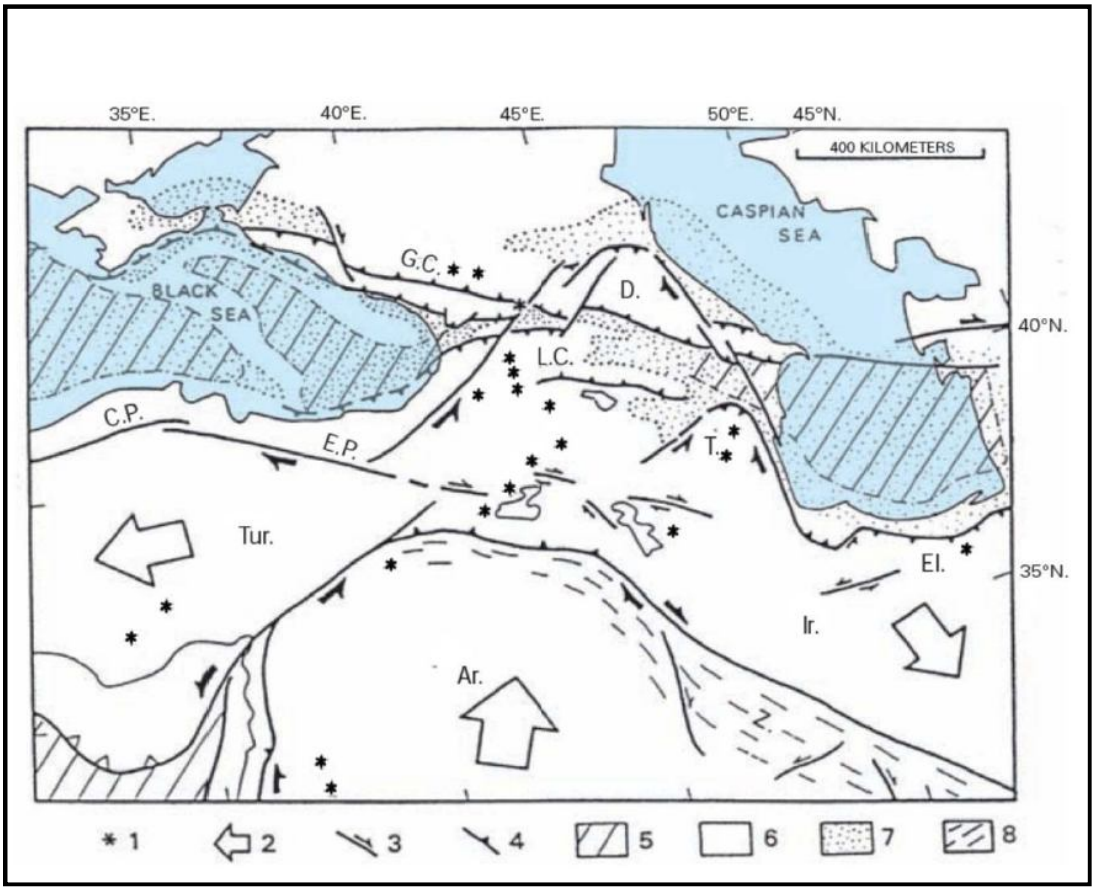


**Figure 3.** Principal tectonic features in the Caspian Sea – Black Sea regions. 1-volcanoes; 2-relative motion of crustal blocks; 03-major strike-slip faults (arrows show relative movement); 4-major thrust faults (saw teeth on overriding block); 5-oceanic or intermediate crust ; 6-continental crust; 7-main sedimentary basin; 8-zone of folding. GC=Greater Caucasus; LC=Lesser Caucasus; T=Talesh; El=Elbroz; Ir=Iranian Block; Ar=Arabian Block; CP=Central Pontides; EP=Eastern Pontides; D=Dagestau; Tur=Turkish Block; SCB=South Caspian Basin. Red square indicated study area (Smith-Rouch, 2006).

In the Middle Miocene, uplift of the Greater Caucasus isolated the connection of the Caspian and the Black Sea, and led to the produced of anaerobic conditions in the basins (Smith-Rouch et al., 2006). Clastic accumulation was dominant during this time period. The plate's interaction in the Greatest Caucus area caused large amounts of sediments influx, in the form of proximal and distal flysch. The sedimentation rate exceeded subsidence, thus filling the basins. By the Middle Miocene, the Caspian Sea was separated from the World Ocean (Golonka et al., 2002). This separation during the Oligocene-Early Miocene time resulted ideal environment for deposition and preservation of organic-rich shales.

During the Pliocene time the strongest subsidence occurred in the basin, when more than 8000 to 10000 meters thick sediments got deposited in that time (Safarov et al, 2007). The South Caspian Basin was isolated from the Middle

Caspian Basin, and was a single lake during the deposition of the Productive Series (Dumont et al., 1998). Isolation of the basin led to the generation of different depositional environment throughout the whole Caspian Basin. The Paleo-Volga River incised a valley in the north which caused a formation of a huge delta in the South Caspian Basin (Nummedal et al., 2002) (Figure. 4). Generally, South Caspian Basin's sediments were deposited in lacustirne environment.

The major transportation agents of sediments were Paleo-Volga, the Paleo Amu- Darya and the Paleo-Kura Rivers (Golonka et al., 2002). There is a compressional structure in the surrounding of South Caspian Basin. It is located between the Caucasus and the Kopet Dag belts, and it is bordered to the South by the Iranian part with the Elbruz belt (Figure 3) (Safarov et al., 2007).

Figure 3 illustrates the position of strike-slip faults and thrust belts bordering the basin and arrows shown the northward migration of the Arabian plate, the southeastward movement of the Iranian block, and the southwestward movement of the Turkish block (Smith-Rouch et al, 2006). First touch of the north most part of the Arabian plate with materials of other continent appears to have started 45 million years ago (Salamov et al, 2005). The main deformation did not begin until the Pliocene in the folded belt of the Zagros Mountains (Falcon et al., 1974).

The basin consists of the region's thickest sedimentations and is bordered by mountains. Those sedimentations mainly got deposited after Oligocene time when foreland basin setting was dominant. A big muddy sequence called Maykop which is also considered significant source rock for the region was deposited Oligo-Miocene (Simmons et al., 1997). The basin was restricted and was related with a dramatic fall in sea level during end of the Miocene. Maykop shale formation was overlaid by sand bodies that were carried to the basin by the Paleo-Volga, Paleo-Kura and Paleo-Amu Darya rivers (Figure 4).


**Figure 4.** Major Delta Systems in South Caspian Basin. (Krooneberg et al., 2005)

These Lower to Upper Pliocene fluvial deltaic sandstones, known as the "Productive Series" (Figure 5), are about 8 km thick and were deposited about 1-2 million years ago. They comprise the main petroleum bearing rocks in the area (Reynolds et al., 1998).

There are several folds corresponding Late Pliocene which are common throughout the basin (Devlin et al.,1999).

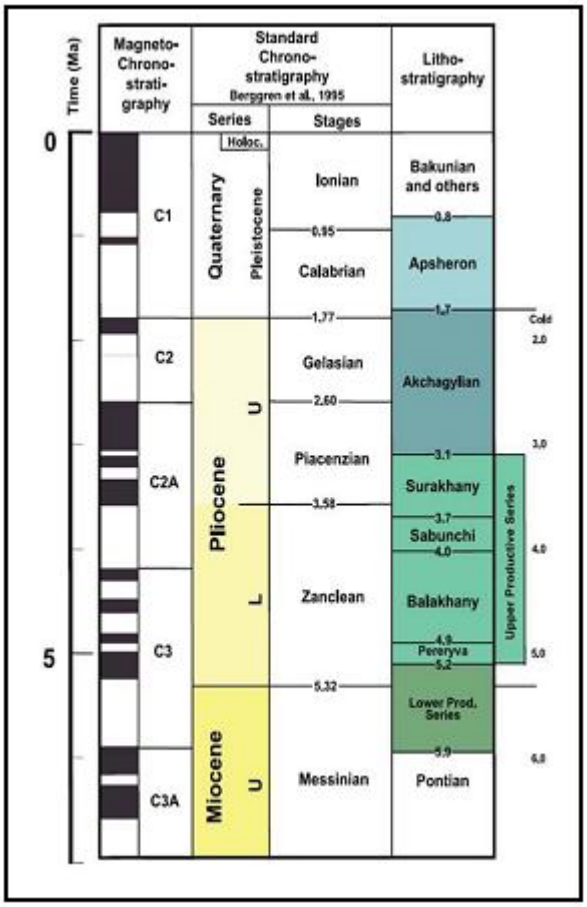


**Figure 5.**Chronostratigraphy of the Upper Miocene to Quaternary formations in the South and Central Caspian basins. (Abreau and Nummedal 2007)

The Productive series are non-marine, deltaic fluvial sediments deposited during the Pliocene. A huge amount of clastic sediment was carried into the basin by the Paleo-Volga, Paleo-Kura and Paleo-Amu Darya rivers running into the Caspian Sea.

High rates of sedimentation and rapid sediment accumulation caused over pressuring of the underlying mud, which are now presently represented as mud volcanoes. Hydrocarbon traps were produced after deformation of the productive series, with the folds detached in the underlying highly pressured mud formation. Generally folds correspond to late Pliocene and younger times through the basin (Safarov et al., 2007).

## 3.2 Stratigraphy of the study area

The stratigraphic subdivision of the South Caspian has been established on the basis of available outcrop studies, cores and logs from deep wells on the western and eastern margins of the Basin (Buryakovsky et al., 2001). Most of the sediments deposited in South Caspian Basin during Early Pliocene time. The Pliocene Productive Series (Figure 5) is the important unit of the essential petroleum interval in the Basin. Formation of this unit is predicted to be established by a main fall in the base level following the absolute separation of the South Caspian Basin from the global ocean during Late Miocene (Hinds et al., 2004; Reynolds et al., 1998). This hydrocarbon bearing unit is about 8 km thick bedding of fluvio deltaic deposits, accumulated at very high rate of sedimentation (2-4 mm/y) because of the Paleo-Volga, Paleo-Kura and Paleo-Amu Darya Rivers (Figure 4), between 5.2 and 3.1 Ma ago (Jones and Simmmons, 1996; Reynolds et al., 1998). The Productive Series has been analyzed by the lithological point of view by examining samples from outcrop, and cores and logs from deep wells. The sediments are lack of fauna and their stratigraphic position is defined by faunal features of the overlying Akchagylian Stage and underlying Pontian Stage. Subdivision of the thick hydrocarbon bearing unit was performed based on changes in lithology which has been resulted from cyclic deposition (Buryakovski et al., 2001). In South Caspian Region, stratigraphic sequences are divided into "suites" rather than formations. It should be noted, that the Russian use of "suite" is equivalent to "formation" in that both are mappable stratigraphic units (Smith- Rouch et al., 2006; Reynolds et al., 1998).

Precise detailed description of the Productive Series largely based on the field work studies of several outcrops around Apsheron Peninsula (Reynolds et al., 1998; Hinds et al., 2004; Kroonenberg et al., 2005).

In the study area the Productive series has been subdivided (Uskin et al., 1916) for 9 subdivisions (Figure 6) because of lithology and their characteristics. These suites or formations and subunits of formations or members are easily recognizable on logs data, and are accepted to be approximately same to regionally mappable units. Despite weak biostratigraphic marks, lithostratigraphic correlation of individual formations has been used. This led Reynolds et al. (1998) to think about the chronostratigraphic significance of individual formations. Moreover, the Productive Series subdivided into two parts: lower and upper parts, with the bottom boundary of the Pereriv Formation (Hinds et al., 2004) (Figure 6).

There are two intervals in Productive Series: 1) Lower part of the Productive Series; 2) Upper part Productive Series. Each interval is subdivided into a number of formations (Uskin, 1916; Azizbekov, 1972; Reynoldset al., 1998). Integration of subsurface and outcrop data suggests that these formations approximate to chronostratigraphically significant packages, which is correlatable over large distance areas (Safarov et al., 2007).

The Lower Productive Series contains five formations:

1. Kalin Formation (KaS)
2. Pre-Kirmaky Formation (PK)
3. Kirmaky Formation (KS)
4. Post-Kirmaky Sand Formation (NKP)
5. Post-Kirmaky Clay Formation (NKG)

The Upper Productive Series contains the following:
1. Pereriva Formation (also may appear as Pereryv, Pereryva)
2. Balakhany Formation
3. Sabunchi Formation
4. Surakhany Formation

Among those suites Kalin Formation (KaS) is the only formation that is not outcropping in any area within Apsheron Peninsula. It is only recognized from the subsurface where it shows coarse-grained conglomeratic succession more than 300 m in thickness and therefore did not illustrate in Figure 7 (Abramovich and Mekhtiyev, 1954).

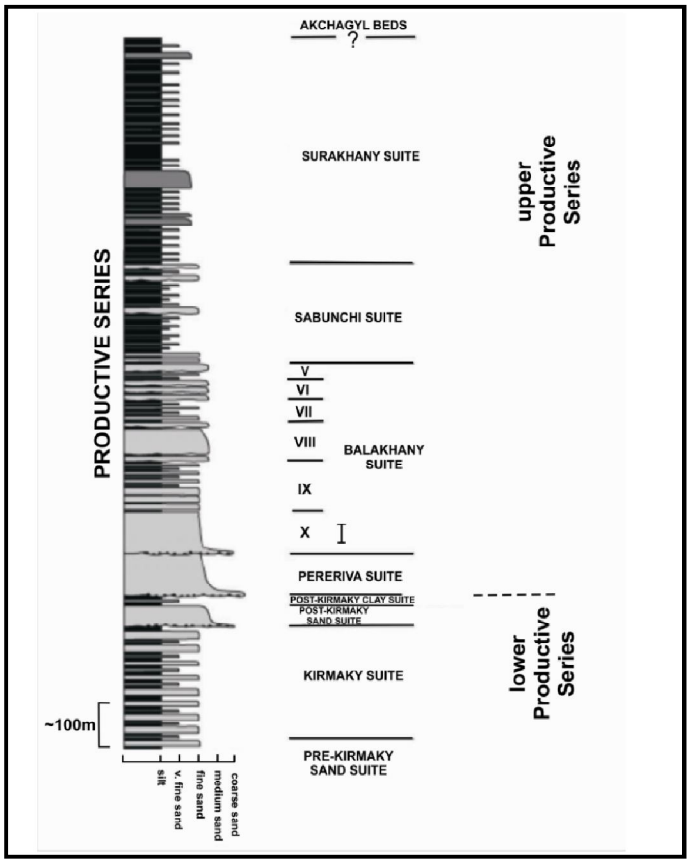


**Figure 6.** Stratigraphic column of the Productive Series. Grey color represented sands, black color mudstone. (Hinds et al., 2004)

The Pre-Kirmaky Formation (PK) is locally more than 150 m thick across the Apsheron Peninsula and characterized by fining-upwards profiles up to 5m in thickness with very coarse sandstone in the base of it which is followed upwards through fine sand to thin-bedded silt and clay.

The Kirmaky Formation (KS) is approximately 250-300m in thickness and is divided into a lower sandstone part and an upper argillaceous part. It indicates a large-scale vertical sedimentary architecture with variations of packages of mudstone and sandstone with changing

thickness between 2 and 8m. Horizontally, these packages exhibit sheet like geometry in dip section, and can be recognized as a consistent form more than hundreds of meters, showing just very little change in. Paleocurrents are basically to the SSE (Reynolds et al., 1998); Hinds et al., 2004).

The Post-Kirmaky Sand Formations about 35-40 m and consists of amalgamated, fining-upward, channelized sandstones with thickness between 2-4 m, and shows an overall fining-upwards trends Paleocurrents are mostly to the SSE (Hinds et al., 2004).

The thickness of the Post-Kirmaky Clay Formations 30-35 m thick and is weakly exposed. The formation is characterized by red to brown, and grey silt with thin, black plastic clays, interbedded with laterally continuous, climbing ripples laminated sandstone and represented by a gradational base with Post-Kirmaky Sand Formation. In some of the horizons desiccation cracks can be seen. There was no clear indication of coarsening upward or fining upward patterns observed within the unit. Paleoflows are dominantly to SSE (Figure 7) (Hinds et al., 2004).

The Pereriv Unit is among the most significant producing formation of the South Caspian Basin. It's about 110m thick and exhibits an overall fining-upward grain-size trend, with quartz conglomerates at the base overlain by mostly amalgamated, broad, channelized sandstone deposits of 2 to 5 m thick with thin siltstone interbeds. Sandstones are represented by different colors from grayish to yellow/brown, to red (Hinds et al., 2004). Fining-upward successions, 4-7 m thick, are common and are characterized by cross-beds up to 3.5 m high (Reynolds et al., 1998). Paleocurrents are mostly to the SSE (Figure 7).

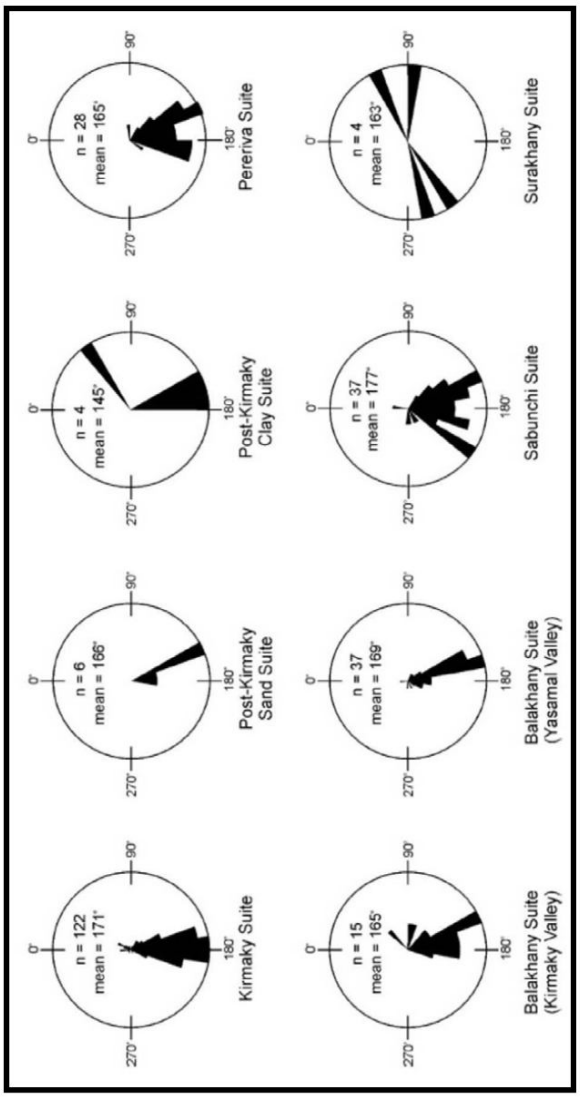


**Figure 7.**Palocurrents of the Productive Series (Hinds et al.,2004)

Another main reservoir formation called Balakhany Formation which is approximately 300 m thick located on the Apsheron Peninsula and is important producing zone in the offshore. It is also divided into 6 subunits (subunit X at the base to subunit V at the top) in which the even-numbered successions represent more sandstone dominated intervals and the odd-numbered ones are mud dominated. The Balakhany X subdivision is about 80m and consists of channelized, cross-bedded sandstone 2 to 5 meters thick showing different amount of amalgamation. Balakhany X subunit exhibits a fining upward trend starting basal conglomeratic sandstone at the bottom to fine sandstones at the top. Color of the sandstones in subunit varies from brown to yellow and orange. The Balakhany IX is about 50 meters thick and it is outcropping in the Yasamal Valley. The lower part shows alteration of channelized, amalgamated sandstone with grey and dark brown mudstone. Mudstone bedding is horizontally consistent for 100 m to 3 m in thickness. Sand filled desiccation cracks can be noticed in some intervals.

The Balakhany VIII subunit is about 50 m in Kirmaky Valley and is nearly 80 m in thickness in Yasamal Valley outcrops. Subunit VIII shows identical sedimentary architecture to subunit X and is characterized by amalgamated, channelized sandstone 2-5 m thick and alterations in color from brownish and grey to yellow. The Balakhany VII subunit is 50 meters in thickness and consists of planar, fine grained, channelized sandstone of 1.5 to 3 meters thick. Those sandstone units are interstratified with poorly established, coarsening upward, mudstone to sandstone, from 4 to 6 meters of thicknesses. In some intervals the reddish-brown mudstones comprise numerous desiccation cracks. The Balakhany VI subunit is about 40 meter thick and is characterized by fine-grained channelized sandstones 6-9 m in thickness. Color of the sandstone varies form grey to yellowish brown.

Mostly amalgamated channels are from 3.5 to 4 meters thick and up to 45 m wide. The Balakhany V subunit is 50-60 m in thickness and consists of sandstone 4 m thick. In this subunit coarsening-upward successions are common (Hinds et al., 2004; Kroonenberg et al., 2005). Paleocurrent for the Balakhany Formation are generally towards the S-SSE (Figure 7).

The Sabunchi Formations approximately 220m thick. Formation is represented by decimeter thick beds of sandstone, mudstone and siltstone. The most part of the succession comprises vertically stacked coarsening-upward, interbedded sandstone and siltstone packages between 4 and 6 meters thickness. They are grayish and yellowish in color. The lower unit of the formation can be recognized with a prominent grey-colored mud, and a sandstone channel recognized as the upper contact. Paleocurrent vectors show a SSE trend (Figure 7), some westerly flows were found (Hinds et al., 2004).

The upper most of lithostratigraphic unit of the Productive Series is Surakhany Formation which is approximately 500 meters in thickness in outcrop. This part is highly argillaceous full of by thick bedded of clay and siltstone, and some amount of sand. Multicolored mudstone packages between 5-25m thick comprising mainly of massive or well laminated claystone and siltstone. Sub-vertical burrows and root traces noticed in siltstone (Hinds et al., 2004). Paleocurrent directions show from ESE to SSW.

Reynolds et al. (1998) suggested modern prediction of deposition environment of the Productive Series which are outcropping around the Caspian Sea, which are very similar to their offshore part of the Apsheron Peninsula. The Reynolds et al. (1998) conducted new interpretation of the area and in his new depositional model for the Productive Series was based on the determination in outcropping sections of mainly fluvial dominated delta facies related of fluvial, delta plain, proximal delta-front and distal delta-front environments that has been interpreted to have genetic relationship with each others.

Reynolds et al. (1998) analyzed the variations of sand and mud rich lithofacies, which represent the Productive Series, as characterizing the repeated juxtaposition of proximal and distal fluvio-deltaic environments. Reynolds et al. (1998) suggested that an extensive braid-delta built southwards across the Apsheron Ridge on a very low-gradient slope into a relatively permanent, though fluctuating, South Caspian lake. According to his model, thick amalgamated channel sand packages are braided fluvial channel deposits, while coarsening-up packages are distributary mouth-bar sands. The thick braided-river sand intervals are related to lowstands in lake level, involving progradation of the delta and a basinward shift of discrete facies belts, whereas rising lake level led to transgression and deposition of widespread highstand mudstones.

Hinds et al. (2004) proposed new depositional environment interpretation of the Productive Series based upon extensive outcrop observations. Formation of the lower part of the Productive Series is thought to be variation of sheet flood related river sediments, channelized deposits and lacustirne muds.

Hinds et al. (2004) interpreted deposition of the "Upper Productive Series as terminal fluvial system which repeatedly expanded and contracted across its alluvial plain, but experienced only moderate lacustrine influence.

Hinds et al. (2004) model proposes that dryness created in desiccation of the lake and a slow background deposition of clays and silts due to the rivers had run dry and little coarse sediment reached the basin (Figure 8A). Hinterland mountains rejuvenation of the river systems during the wet periods dumped large volumes of coarse erosion products into the basin during flashfloods that were reworked by the ephemeral braided streams on a low-gradient fluvial lacustrine enlargement and ubiquitous deposition of muds and silts in shallow water was initiated by the increasing river flow. High frequency climatic cycles are thought to be responsible for individual sand units, while longer term cycles of ~100,000 year produce the sand packages and thicker mudstone units (Figure 8D). In this model, reservoir sand-bodies were deposited over large parts of the basin at the start of humid periods just before lake levels began to rise and are predominantly braided-river channel-fill (amalgamated channel sand packages) and prograding sheet-flood overbank lobes (coarsening-upward packages).

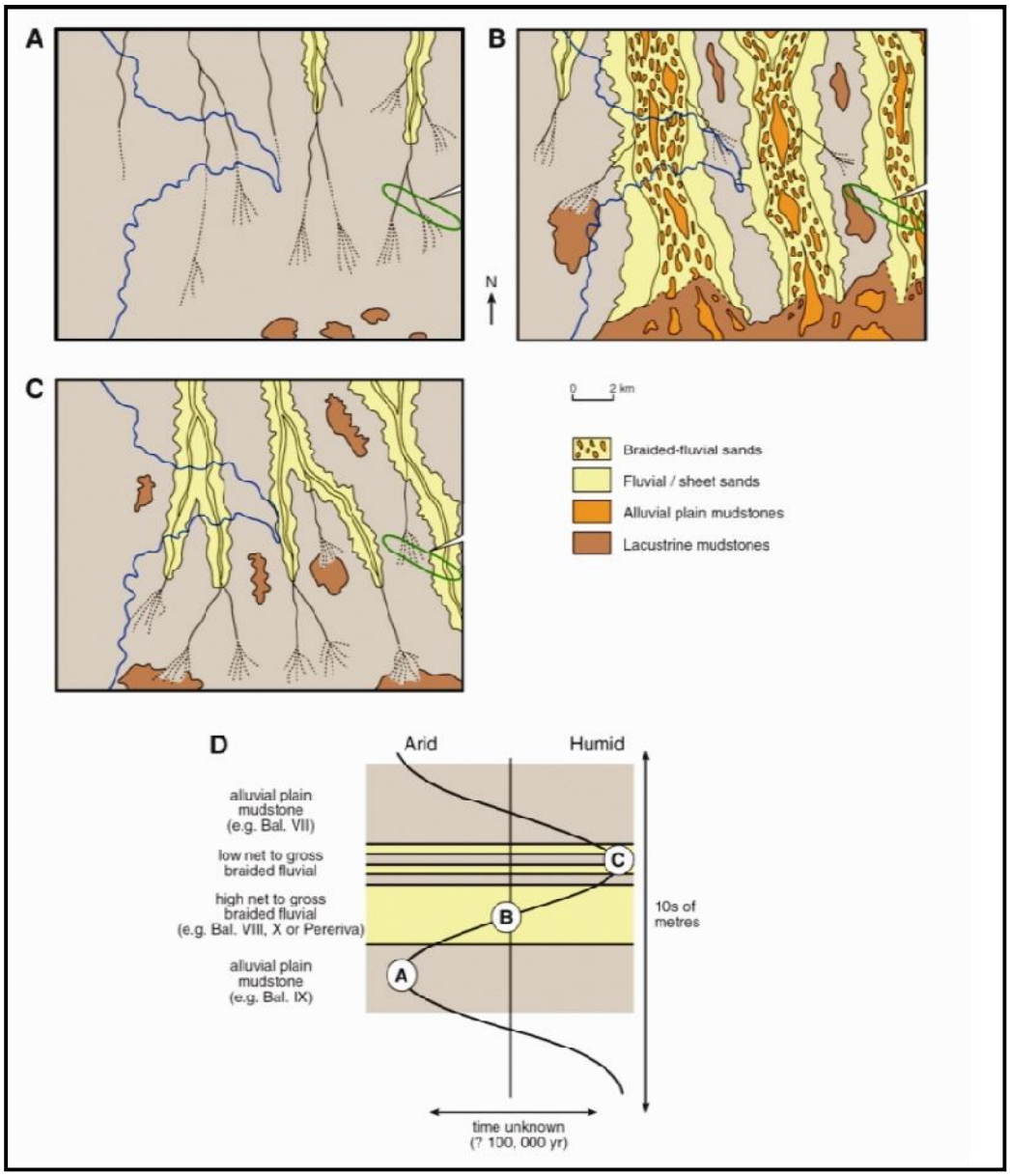


**Figure 8.** Paleogeography of the Productive Series on the Apsheron Peninsula and surrounding areas during: (A) maximum aridity and minimum coarse clastic and water input; (B) increasing climatic humidity and establishment of sand – rich braided river systems possibly feeding a braid – delta further south; and (C) declining sediments load produces low – sinuosity sand – poor braided fluvial systems. (D) Climatic cycle that could have driven the depositional environments of the Productive Series. Green ellipsoid represents the position of study area (Hinds *et al*., 2004).

## 3.3 Field background

Azeri-Chirag-Guneshli (ACG) is huge offshore oil filed in South Caspian Basin, approximately 120 kilometers away from the shoreline of Caspian Sea – Apsheron peninsula sector. Area of the field is about 432square kilometers. It is operating ten different petroleum companies (consortium) leaded by BP. Azeri-Chirag-Guneshli fileds have been estimated recoverable hydrocarbon of about 6 billion barrels. As of the end of 2005, the production rate from eight drilled wells at the platform was approximately 240 000 barrels per day. The peak of oil production over 800000 barrels per day, was obtained in third quarter of 2010. In the beginning of 2012 oil production was about 710000 barrels per day.

The structural trap, which forms the huge oil field, is a North West-South East trending, trusted anticline with steep dip angle. Within this structural closure there are several crestal faults cut in strike direction as well as mud volcanoes of different size that makes the structure complex. Oil and gas are observed within a number of various zones corresponding to Pliocene time; the most significant reservoirs encounter in the Pereriv and overlying Balakhany Formations. The high oil column that characterizes the field is the result of extensive structural relief combined with excellent top and lateral seals, for example, 900 meters on the north part of Azeri and 580 meter on the south of Chirag. Varying pressure regimes linked with effective seals may be responsible for the greater than 300 meters north-south alteration in oil contact(s). At the main Pereriv reservoir level, the ACG Field is 50 km in length and 5 km in width.

Hydrocarbons are explained to have been generated and migrated from Late Miocene to Early Pliocene aged Maykop lacustrine shale buried in the deep and rapidly subsiding South Caspian basin to the south of ACG. The ACG anticline was originated in the Late Pliocene in response to compression related with the formation of the Alpine/Himalayan mountain belts to the south. Release of highly pressured, deeply buried shale exploited lines of weakness associated with the inversion and faulting forming a number of mud volcanoes some of which are still active.

# CHAPTER4

# METHODS AND APPLICATIONS

For identification of petrophysically based reservoir zonation and characterization, the appropriate representative data of the studied reservoir must be acquired. The relevant methods for getting such data can be listed as (1) conventional core plug tests, (2) well logging. In this section, the methods and their applications; which are utilized to build a hydraulic flow unit zonation within the reservoir of scope Azeri-Chirag-Guneshli filed), are described that uses the available data. The approach tried to be applied in the study comprises the fundamental geologic framework of the area of intereset, the petrophysical features of ACG field, interpretation of core-plug data, analyses of well logging data, combination of all these works to get a hydraulic flow unit zonation with the help of permeability/permeability estimation in the logged but uncored well.

## 4.1 Available data

There are 9 cored wells with log data and 12 noncored with log data in Azeri Chirag Guneshli filed in order to divide the field into the flow units. Conventional core analyses were utilized and small database has been constructed based on the result of those analyses. The wells which have core and log data are A08Z, B01ST1, C01, D01Z, GCA1, GCA2, GCA4, GCA4Z, GCA5, GCA5Z, and GCA6. Figure 9 is a map which shows the well locations. These wells have both core and well log data. The core analysis produced several parameters and those parameters are categorized into 3 division: Petrographic consolidation, Pc parameters, RCAL data.

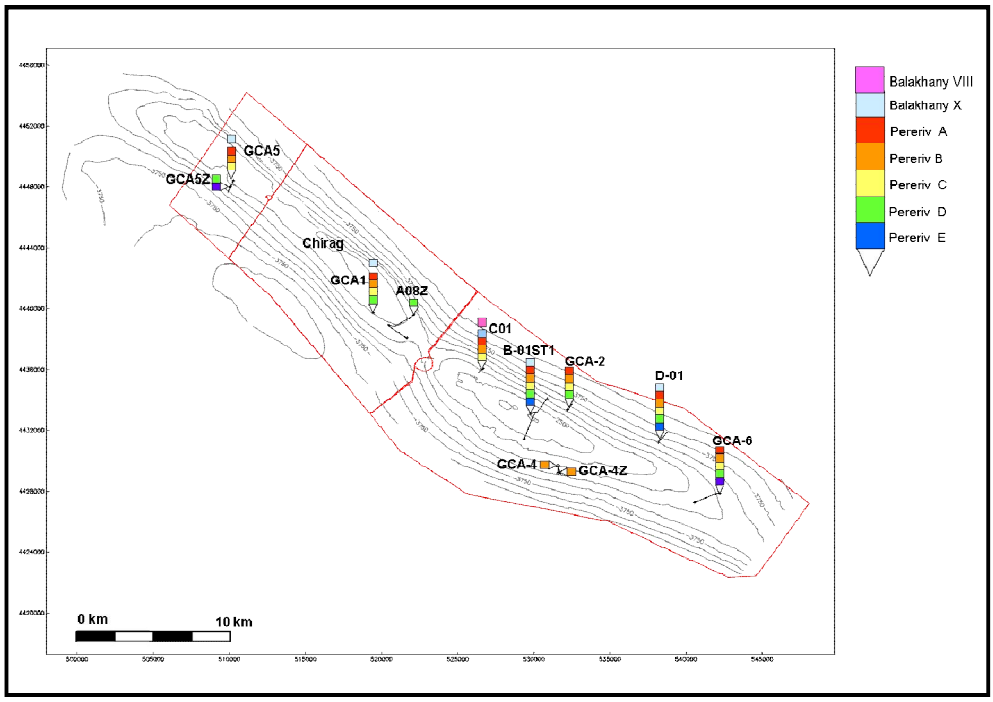


**Figure 9.** Area of interest (Structural map) with well locations and formations.

These 3 main data categories have also been divided into subdivisions. Subdivisions of petrographic data include: sandstone classification, textural data (mean grain size, sorting), framework grains (%), ductile components (%), authigenic minerals (%), modal porosity (%), ICCS Hg porosimetry analysis (Hg porosity, hydraulic radius, Hg permeability) and permeability porosity data from core analysis under 400PSI. Pc parameters include: porosity of helium and hg, permeability of air and hg, pore throat sorting and radiuses.

Moreover, besides these core parameters there are conventional well logs. Usually, GR, caliper log, sonic, deep and middle resistively, neutron, density were utilized in the wells.

Table 11 below briefly summarizes available data for the project of flow units.

**Table 1.** Available core and well log data

| Core Data | | | Well logs |
|---|---|---|---|
| Petrographic Consolidation | Pc Parameters | RCAL | |
| Sandstone classification | PORhg (%) | CPOR | DEN |
| Mean grain size | PORhel | CKHEL | CALI |
| Sorting | Fpurcell | | GR |
| Fraimwork Grains (%) | Kair | | NEU |
| Ductile Components (%) | Khg | | PHIE |
| Authigenic Minerals (%) | PTS,psi | | PHIT |
| Modal porosity (%) | Rapexavto | | RESDEP |
| ICCS Hg porosimetry | Rparachor | | DESMED |
| | Rapexman | | SONIC |
| | Sapex | | SW |
| | r5-r85 | | VSHALE |
| | Rariphimetic | | |
| | Rweighted_aripmetic | | |
| | Rgeometric | | |
| | Rweighted_geometric | | |
| | Rharmean | | |

All of these data sets have been taken from BP and Confidentiality Agreement. This Agreement is entered into as of 01 February, 2013 ("Effective Date"), between Middle East Technical University ("University") having established under the laws of the Republic of Turkey, having a registered office at METU Üniversiteler Mah., Dumlupınar Blv. No:1, 06800 Çankaya Ankara/TURKEY ("University"), BP Exploration (Caspian Sea) Limited, a company organized and existing under the laws of England, and represented by its duly registered Representative Office in the Republic of Azerbaijan, having its registered address at Nizami 96, Baku AZ1010, Azerbaijan ("BP") and Rahim Rzazade Ramiz, holder of passport AZE no.05890084 issued on 26 May, 2006 with his registered address at Inshaatchilar ave.38 apt.22, Baku/AZERBAIJAN and currently residing at 100.Yil, Ishchi Bloklari 1535, 218/2 Ankara/TURKEY ("Student") ("Agreement"). University, BP and Student may be individually referred to as "Party" and collectively as "Parties".

Whereas, BP is willing, in accordance with the terms and conditions of this Agreement, to disclose to Student and University scientific, technical or other information which is considered by BP to be proprietary and confidential ("Confidential Information"), as further defined below for the purpose of Student's academic research and thesis development at the University ("Thesis").

"Confidential Information" may include, but is not limited to, biological materials, computer source codes, diagrams, electronic files, trade secrets, theories, methods,

material composition, invention disclosures, patent applications, technical and scientific information, research data, draft publications, technical reports, research plans, business plans, financial reports, projection and agreement terms provided by BP to the Student and University.

The Parties have hereby agreed that:

1. In consideration of the disclosure referred to in Paragraph 2 hereof, Student and University agree that Confidential Information and Thesis shall be kept confidential and shall not be sold, traded, published or otherwise disclosed to anyone in any manner whatsoever, including by means of photocopy, reproduction or electronic media, without BP's prior written consent.
2. Confidential Information shall only be used by the Student and University for Thesis purpose.
3. Confidentiality obligations and limitations on use set forth in this Agreement shall become valid from Effective Date.
4. Disclosure of Confidential Information, Thesis and the execution of this Agreement shall not be considered to grant a license nor conveyance by BP of any intellectual property rights including those rights under any patents or patent applications. None of the present or potential patent rights of BP in existing Confidential Information shall be affected by this Agreement. Confidential Information shall remain the property of

   BP and no rights are granted to the Student and the University except the limited right to use Confidential Information as set forth above.
5. This Agreement shall be governed by and interpreted in accordance with the substantive Laws of England. Any dispute arising out of or relating to this Agreement, including any question regarding its existence, validity or termination, which cannot be amicably resolved by the Parties, shall be settled before a sole arbitrator in accordance with the rules of London Court of International Arbitration in England. A dispute shall be deemed to have arisen when either Party notifies the other Party in writing to that effect.
6. Each Party shall be fully responsible for any damages and losses caused to the other Party as a result of breach of this Agreement.
7. No amendments, changes or modifications to this Agreement shall be valid except if the same are in writing and signed by a duly authorized representative of each of the Parties hereto.

### 4.2 Well Logging Data Analyses

Surface geological techniques are able to identify subsurface structures which could possibly contain fluids inside it; however, they can not to predict if this fluid is hydrocarbons. So far, there is no possible way than drilling a well to exactly determine the presence of hydrocarbons in subsurface. Whereas, to drill a well is money and time consuming process, that end with a result of none hydrocarbon bearing zone in the drilled sections. However, more relevant way is to use the formation evaluation tests for analyzing the interested subsurface zone, rather than drill a well. Formation evaluation is the procedure of working on drilled well measurements to evaluate the characteristics of the subsurface reservoirs, such as identification of the physical and chemical features of reservoirs and their contained fluids.

There are 4 method of formation evaluation: (1) core analysis (2) drillsteam test (3) mud logging (4) well logging. One of the easiest ways of obtaining subsurface data at the early stage of the study can be considered as well logging, which chiefly contributes to formation evaluation. The main aim of the well logging is to recognize the reservoir rocks, calculate the hydrocarbons in place, and estimate the recoverable hydrocarbons; beside these the data acquired from well loggings also contribute so many.

In Azeri-Chirag-Guneshli field, the conventional open-hole well logs are available as mentioned above. These log data are used to study the lithological-mineralogical components and the petrophysical parameters like effective porosity and fluid saturations. As well as the use of raw log data, some cross plots can be also utilized based on log parameters which are used to understand the nature of porosity. Acquired well log elements are also run as input for the geostatistical methods, for correlating with core data for permeability/porosity estimations. The way of evaluation methods on well logs and the applications of these methods to the worked wells will be described in this part.

#### 4.2.1 Gamma Ray Analysis

The recognition of shaly rocks (formations containing clay minerals) can be done by using mainly Gamma Ray (GR) Log. Spontenous Potential (SP) Log can also be used for this purpose. Two elements which are radioactive, Thorium (Th) and potassium (K) tend to exist in shales. Shale-free sandstones and carbonates (usually considered as *clean zones*) contain very little amount of K and Th, because the chemical environment that dominate during their accumulation is not favorable for the deposition of radioactive minerals. In GR logs, the important abundance of unstable elements, show a certain level of natural radioactivity. The GR log's a measure of the overall gamma radiation the well that is used to recognize probable petroleum bearing reservoir rock and shales.

Shaly zone of the formation can be described as shale volume (Vsh). Qualitatively, Vsh shows whether the zones areshaly or clean. Quantitatively, Vsh helps to know the shale effect on log responses and, if needed, to correct them to non shale formation responses by means of cross plots.

Volume of the shale can be estimated by using the following equation

$$V_{sh} = \frac{GR_{\log} - GR_{clean}}{GR_{shale} - GR_{clean}} \quad (1)$$

GRlog = gamma ray response in the zone of interest
GRclean = average gamma ray response in the cleanest formations
GRshale = average gamma ray response in shale

Well GCA1:

The GR log for well GCA1 is available from 490 m - 2958m. In this well the zone of interest (Pereriv B) penetrates in 2764 meters and the bottom of the formation is in 2804 meters. Generally this zone is clean sandstone with few amount of shale content. That is reason why this is is one of the prolific hydrocarbon bearing zone.

Well GCA2:

The GR log is available for 353 – 3647 meters in GCA2 well. The interval of interest for this well is being penetrated in 3243 meters. Also bottom of the formation is in 3300 meters. The well GCA2 is also shows low Vshale value throughout the Pereriv B zone although there is very few thin shale zones.

Well GCA4:

The GR log is available for 2370 – 3467 meters. Well GCA4 hit the formation Pereriv B in depth of 3108 m. Bottom of the formation is in 3159 meters. The interval is clean sand with thin shale layers.

Well GCA5:

The GR log is available for 268 – 3030 meters. Well GCA5 hit the formation Pereriv B in depth of 2888 m. Bottom of the formation is in 2936 meters. As other wells in the area GR responses shows low value for Pereriv B.

Well GCA6:

The GR log is available for 703 – 3471 meters. Well GCA4 penetrates the formation Pereriv B in depth of 3333 m. Bottom of the formation is in 3377 meters. The interval is clean sand with very thin shale layers.

Well C0-1:

The GR log is available for 90 - 3011meters. Well C0-1 penetrates the formation Pereriv B in depth of 2816 m. Bottom of the formation is in 2903 meters. The interval is clean sand with thin shale layers.

Well D-01Z:

The GR log is available for 1388 – 3889 meters. Well D-01Z penetrates the formation Pereriv B in depth of 3740 m. Bottom of the formation is in 3796 meters. GR responses in this well show that the well is highly sandstone zone with thin shale content.

Well B01ST1:

The GR log is available for 171 - 2504 meters. This well penetrates the formation Pereriv B in depth of 2366 m. Bottom of the formation is in2411 meters. The interval is clean sand with thin shale layers.

Well A08Z:

The GR log is available for 1118 – 3822 meters. Well A08Z hits the formation Pereriv B in depth of 3611 m. Bottom of the formation is in 3695 meters. The interval is clean sand with thin shale layers.

**4.2.2 Sonic Log Analysis**

Sonic log is a significant way of formation analysis. This type of logging uses the acoustic wave propagation around the well bore. As the log responses are not changed by secondary porosity, they may be used to correlate within wells. Sonic logs generally help to estimate porosity. Two ways are described for porosity estimation from sonic logs; Wyllie Method and experimental method.

Conventional sonic log measure the reciprocal of the velocity of the compressional (P wave) wave. This value is called interval transit time, Δt, or slowness, and its unit is microseconds per foot (μsec/ft). Porosity of consolidated formations is related to Δt by Wyllie's equation.

$$\phi = \frac{\Delta t - \Delta t_{mat}}{\Delta t_f - \Delta t_{mat}} \quad (2)$$

Where;
$\Delta t_{mat}$ and $\Delta t_f$ are the slowness of the matrix and pore fluid respectively, and Δt is the slowness of the zone of interest.

The average values of matrix for Wyllie's equation are stated below.

**Table 2.** Matrix velocities used in Wyllie's Equation

| matrix type | Δtmat(μsec/ft) |
|---|---|
| Sandstone | 55.5 |
| Limestone | 47.5 |
| Dolomite | 43.5 |
| Fluid | 189 |

The sonic porosities of the wells are acquired by using Wyllie's equation. The porosities obtained from sonic log are the primary porosities, but the sonic waves are not measured within the fractures and vugs of the zone in consider.

### 4.2.3 Caliper Log Analysis

Looking at borehole diameter with caliper logging has showed clearly that the actual borehole size often differs from the bit size which is used to drill it.

The difference is significant in some circumstances. Usually, the drilled well is far from being a regular cylinder with uniform size.

The borehole's size and shape depend on the formation drilled. Enlargements of the drilled hole are most commonly seen in shales and shaly formations. (Bassiouni et al., 1994). Due to their electrochemical characteristics, clay minerals absorb water, making the shale formation to swell. Enlargements can also be seen in water-soluble formations, such as salts.

Such kind of enlargements is because of the soft, unconsolidated zones that the drilling mud causing souring effects. In some cases, the hole is looked as it is being drilled smaller than its actual bit size. This is mainly when in permeable reservoir rock drilled with mud that contains solids. This effect which is called mud cakes occur in this sections making smaller diameters.

Such analyses of caliper log measurements require knowledge of borehole diameter and shape. To determine the borehole geometry, caliper log is run with microresistivity, density, sidewall neutron, sonic, and dipmeter logs. Besides giving knowledge about the borehole shape calipers can also be used obtain the permeable zones of the drilled formation.

### 4.2.4 Density Log Analysis

The density log measures the density of the formation rock. If the matrix densities are known, the recorded ρb values can be used to determine the porosity.

The bulk density, (ρb) is the overall gross or weight-average density of a unit of the formation. Solving for porosity yields,

$$\phi = \frac{\rho_{mat} - \rho_{bulk}}{\rho_{mat} - \rho_{fluid}} \quad (3)$$

Where; ρf is the average density of the fluids in pore spaces. Common values of ρma are given in table 3.

**Table 3.** Matrix values for common types of rocks

| rock type | ρ matrix (g/cc) |
|---|---|
| Sandstone | 2.65 |
| Limestone | 2.71 |
| Dolomite | 2.87 |
| anhydrite | 2.98 |

The values for ρf are listed in Table 4.

**Table 4.** Fluid densities according to the mud type

| fluid type | ρ (g/cc) |
|---|---|
| oil | 0.9 |
| fresh water | 1 |
| brine | 1.1 |

The estimation of porosity by using density log applies only to relatively simple environments. In complex environments, such as shaly sands, gas-bearing formations, and complex lithology, the density log is linked with other porosity logs. Porosity estimation gets more difficult when the lithology is not known or when it contains two or more minerals of unknown proportions. The most common mixtures associated in our wells are the combination of shale and sandstone.

Density log are usually applied with neutron log tools and the analysis are based upon both of them. If it is used alone, it is used to know the identification of the formation rock porosity and its bulk density. Bulk density is the sum of matrix density and fluid density.

### 4.2.5 Neutron Log Analysis

The neutron logging is based on the elastic scattering of neutrons as a collision with the nuclei in the target. Target with high hydrogen content shows low concentrations of neutrons, and inversely, target with low hydrogen content shows high concentrations of neutrons. As most of

the hydrogen is part of the fluids located in the porous area, this value is inversely proportional to porosity.

The wellbore size, temperature, mud cake, mud salinity, reservoir pressure, and formation water salinity influence the neutron log measurement, but such changes can be removed by applying some correlation charts. The abundance of gas and shale in the reservoir also affect the neutron logs record. The shale in the formation can result in higher values of neutron porosity. Neutron logs are usually plotted with density logs as mentioned before. Together, they are the most efficient lithology and porosity identification logs besides determination of gas-bearing formations.

The lithology identification is usually based on neutron-density logs. The location of neutron and ρb curves, the separation between them gives lithology understanding.

Neutron logs help to estimate porosity, in fact the actual values of the neutron gives porosity measurement, however, when the density log values are added into the porosity estimations, such as in the density-neutron crossplot technique, the results are more reliable than the neutron and density porosities alone.

The porosity estimated by means of density-neutron can be shown as Ø D-N. This result can be considered to be very identical to the core porosity obtained by laboratory tests.

The Ø D-N porosity is the total porosity of the interval of the interest. This total porosity includes also the ineffective porosity that is already inside it.

Since the irreducible water saturation can be excluded from the production, as saturation calculations are done, this total porosity can be considered as an effective porosity as accepting the error that may occur, or instead Magnetic Resonance (MR) can be used, if available.

The Ø D-N value can be estimated as follows:

- the bulk density number are taken from the log. These values are used to get density porosity (Ø D ) by using the Equation 3.
- the neutron porosity number are taken from the log. Necessary corrections have to be performed for lithology using the chart in Figure 10, to obtain corrected values of neutronporosity (Ø N )
- by using below equation, the Ø D-N porosity is calculated.

$$\phi_{D-N} = \frac{\phi_D - \phi_N}{2} \quad (4)$$

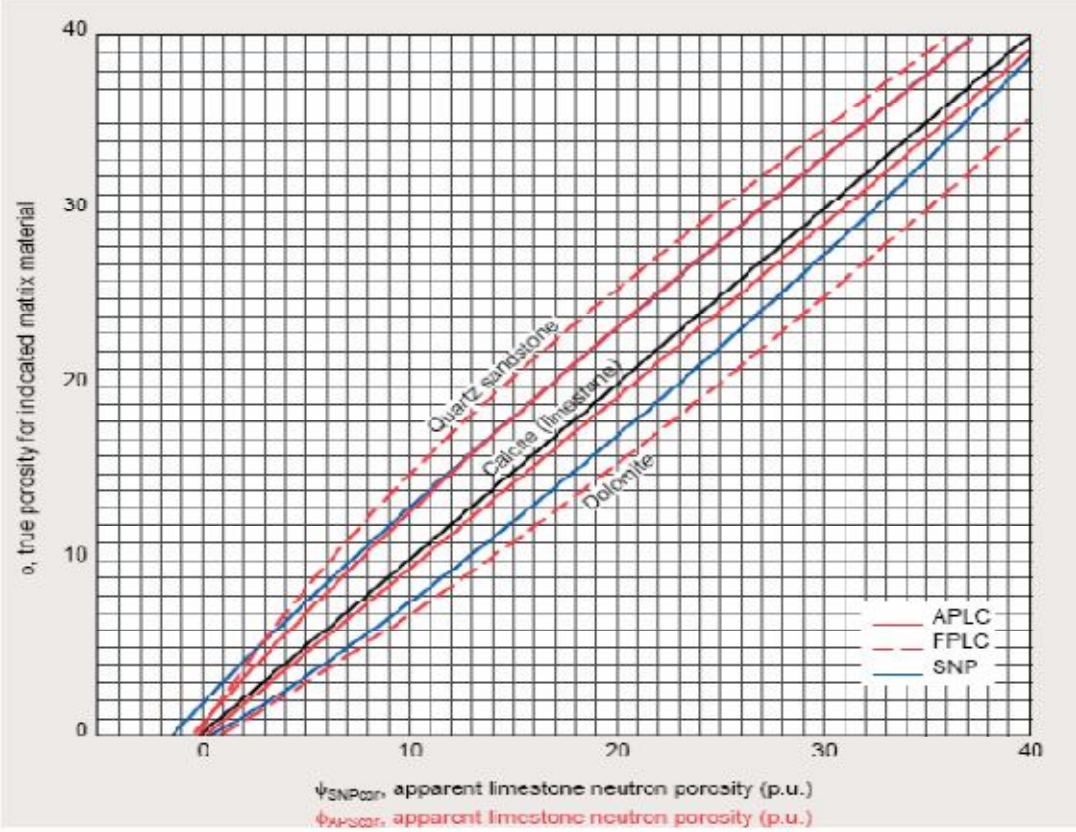


**Figure 10.** Neutron Porosity Equivalence Chart (Schlumberger, Log Interpretation Charts, 1988)

The Ø D-N porosity can also be estimated by means of density-neutron cross plots. The cross plot utilized in most cases is given in Figure11. This cross plot is mainly used for porosity determination. The second purpose of it is to recognize the lithology types in percentages.

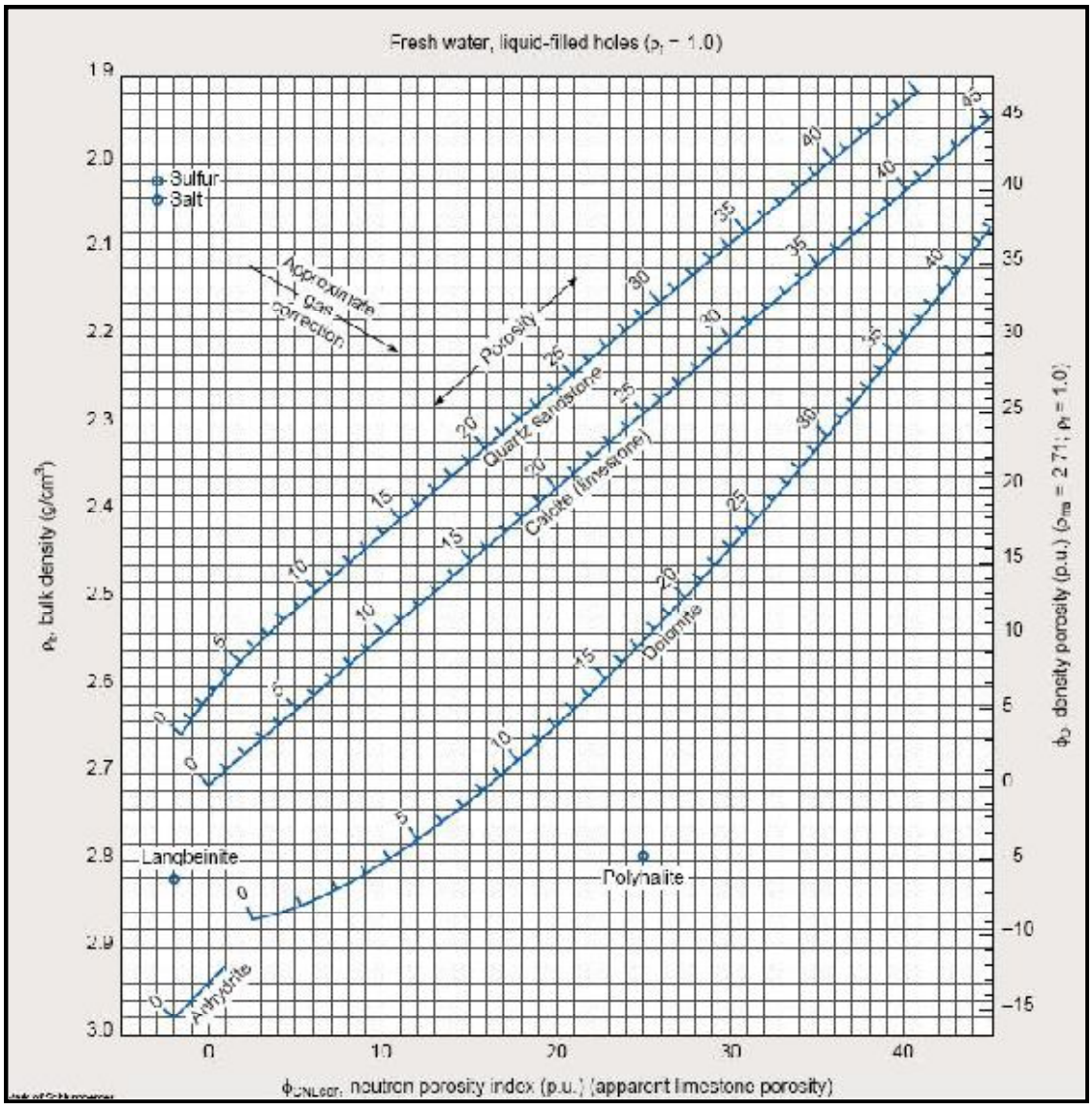


**Figure 11.** Crossplot for Porosity and Lithology Determination from density log and compensated neutron log (Schlumberger, Log Interpretation Charts, 1988)

### 4.2.7 Resistivity Log Analysis

For determining the saturations of hydrocarbons within the formations, firstly saturations of water should be calculated. A resistivity of a reservoir is the ability of its constitients to transmit electricity. The tools used for resistivity logging are classified within depth of investigation as follows;

- Deep resistivity tools for uninvaded zones
- Shallow resistivity tools for transition zones
- Microresistivity tools for flushed zones

The most commom resistivity tools in use can be classified as;

- Dual Laterolog Tool
- Dual Induction Tool
- Micro Spherically Focused Log
- Microlog

The resistivity of a target with its lithology and fluid (water and hydrocarbon) and in the pores is true resistivity (Rt) of the formation. A porous and a permeable reservoir has always water, even it includes hydrocarbon. The water in the pores of formation before it drilled is the formation water saturation (Rw) of the formation. After a drilling operation, drilling mud penetrates and this influences the vicinity of the wellbore forming different zones with different resistivities. This zonation is shown in Figure 12.

The original water saturation, Sw is only valid for the zones of uninvaded formation. The flushed zone is totally invaded with drilling mud with a resistivity of Rmf, and the saturation of this formation is shown as Sxo.

A resistivity of a formation which has saturation of 100% with water (Sw =1) can be called as Ro and the resistivity of the water that saturates the formation is Rw, then there is a ratio between them. This ratio is called "formation resistivity factor" or" formation factor*"* (F).

$$F = \frac{R_o}{R_w} \qquad (5)$$

F is generally controlled by porosity and tortuosity. But, the rock tortuosity is very difficult to record. On the basis of laboratory measurements of F and porosity, Archie proposed the following equation in 1949.

$$F = \frac{1}{\phi^m} \qquad (6)$$

Where, *m* is the cementation exponent

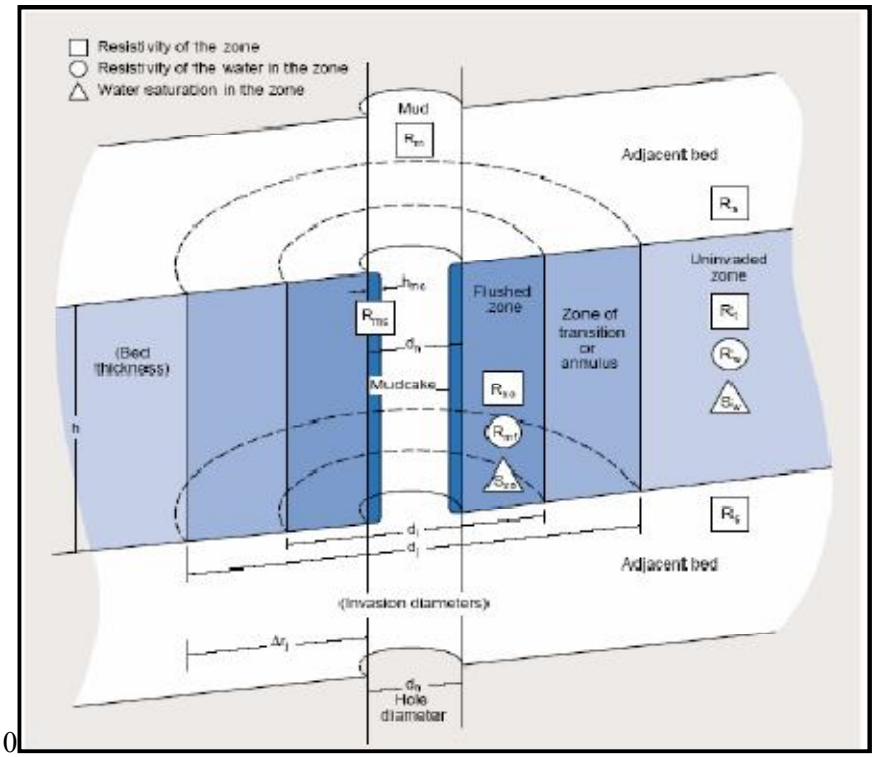


**Figure 12.** The zones around borehole due to mud invasion (Schlumberger, Log Interpretation Charts, 1988)

Another empirical formula relating F and porosity was also proposed by the results of the experiments conducted by Winsaeur in 1952. This equation is in the form of;

$$F = \frac{a}{\phi^m} \quad (7)$$

Where $a$ is the tortuosity constant. The values of a and m vary with pore geometry. The m varies mainly with the degree of consolidation of the rock.

After the calculation of F value, water saturations can be computed by using Archie's Equation as blow;

$$S_w = \sqrt{\frac{R \cdot R_w}{R_t}} \quad (8)$$

Rw is the saturation of water for uninvaded zone, and Rt is the true resistivity of the formation that can be recorded from deep resistivity logs (R-LLD).

Using the same equation, the saturation of water for the flushed zone can also be computed.

$$S_{xo} = \sqrt{\frac{F \cdot Rmf}{R_{xo}}} \quad (9)$$

Where Rmf is the resistivity of the mud filtrate, and Rxo is the resistivity of the flushed zone.

Rxo can be obtained by Micro Spherically Focused Log (MSFL).

The hydrocarbon saturation in the uninvaded zone, which is the oil saturation (So) is then,

$$S_0 = 1 - S_w \quad (10)$$

And the hydrocarbon saturation in the flushed zone, which is the residual oil saturation (ROS) is calculated as;

$$ROS = 1 - S_{xo} \quad (11)$$

The difference between the saturations of invaded zone and uninvaded zones result in movable oil saturation (MOS).

$$MOS=So-ROS \quad (12)$$

In order to find saturations, Rw should be computed.

### 4.2.8 Core Data Analysis

The reservoir characterization has to contain core analyses that allow researchers to know the reservoir parameters such as porosity type, porosity distribution, and permeability. All data obtained from the core data analyses have to be checked carefully and comparisons should be made with other available data. For an efficient reservoir characterization, all available data of core analyses, well logging, and production tests have to be taken into consideration. But usually, not all the wells are cored, because coring is an expensive process, so with the available data in hand, the other parameters are tried to be compared with one another and estimations are made.

Three types of core analyses are commonly used; (1) conventional or core plug analysis, (2) whole core analysis, (3) sidewall core analysis (Helander et al., 1983). The most advanced technology of Core Tomography (CT) is also in use for core analysis.

Commonly core plug method is used. A small plug sample is taken from the core and rock properties such as porosity and permeability are checked. If theheterogeneities exist such as fractures and vugs, the coreplug analysis is not reliable and whole-core analysis is applied.

In sidewall coring, a sidewall core is cut from the wall of a drilled well. In ACG field, there are a lot of conventional core analyses are available. These analyses include coreplug porosities (in %), air and liquid permeabilities (in mD), and grain densities (in g/cc) within related depth intervals.

Firstly the provided core plug data were investigated individually; basic statistics were applied to core data, correlation between the parameters was established.

After a wide study on coreplug data, the measurements were correlated with the results from well logging data to construct estimation models and to understand which parameters are dominant over these models.

### 4.2.9 Core Plug Porosity Analysis

From the reservoir engineering standpoint, one of the most important rock properties is porosity, a measure of the space available for storage of petroleum hydrocarbon (Amyx et al., 1960). Porosity can be divided into subgroups according to its origin; (1) original primary), (2) induced (secondary). Original porosity is developed in the deposition of the material, and induced porosity is that developed by some geological processes after the deposition of rock (Amyx et.al, 1960).

Core plugs commonly do not directly show porosity values that comprise the effects of post depositional events. The methods used for the determination of pore volume and bulk volume are unsatisfactory, because drainage may occur from larger pores (Amyx et al, 1960). It is better to use larger and longer core samples, as in whole core analysis, to estimate the bulk volume. However, this is not always feasible, so the results gained from the core plug should be relied on.

The mean values of the core plug porosity for each wells is shown in Table 5.

**Table 5.** Average porosity (%) values for the wells (Pereriv B)

| GCA1 | GCA4 | GCA5 | C-01 | D-01Z |
|---|---|---|---|---|
| 19 | 16 | 15 | 14 | 19 |

### 4.3 Core Plug Permeability Analysis

The ability of the formation to conduct fluids is known as permeability. The measurement of permeability is a measure of the fluid conductivity of the particular material (Amyx et al., 1960).

Darcy's equation is used to define fluid flow in porous media.

$$k = \frac{Q}{A} \bullet \frac{\mu L}{\Delta P} \quad (13)$$

Where, Q is the flow rate in (cc/sec), A is the cross-sectional area in (cm2), L is the length (cm), ΔP pressure difference in (atm), and μ is viscosity of the fluid in (cp).

Permeability measurements need to be held in care in order to acquire reliable results that represent the reservoir. Permeability can be identified by means of liquid permeability tests or gas permeability tests. In each case, the determined permeability is called as liquid permeability and air permeability(if air is used). If liquid is used, the fluid should not react with the solids in the core sample. As gas is used, gas slippage can be seen, known as Klinkenberg effect. As an example of reaction that can be seen between fluids and solids may be given as clay swelling in the presence of water.

It must also be kept in mind that, when the core is taken out from the reservoir, all of the confining pressures which attribute to overburden pressures are removed. Compaction of the core due to overburden pressure may cause as much as a 60 percent reduction in the permeability of various formations (Amyx et al, 1960).

For ACG field, air and liquid permeability values are available for Pereriv B formation. Average values of permeability are given in table 6.

**Table 6.** Mean permeability values with mD

| GCA1 | GCA4 | GCA5 | GCA6 | C-01 | D-01Z |
|---|---|---|---|---|---|
| 224 | 683 | 452 | 200 | 176 | 351 |

# CHAPTER 5

# GEOSTATISTICAL DATA ANALYSIS

## 5.1Dataset

9 wells A08Z, C01, D01Z, GCA1, GCA2, GCA4, GCA5, GCA6, and B01ST1 were available for the geostatistical reservoir characterization of Azeri-Chirag-Guneshli field.

The simple conventional well logging was used for obtaining better understanding of reservoir parameters. Conventional well logs such as GR, Caliper, Density, Neutron, Sonic, and Resistivity have been run in almost all wells available for this study. Table 7 is a simple example of well (GCA1) log data showing all available digitized well log data for only small vertical section.

**Table 7.**Well log of GCA1 well

| DEPTH M | DEN G/C3 | CALI IN | GR GAPI | NEU V/V | RESDEP OHMM | SON US/F |
|---|---|---|---|---|---|---|
| 2764.7 | 2.47929 | 8.193 | 51.204 | 0.2083 | 9.6955 | 99.16 |
| 2764.8 | 2.46049 | 8.189 | 49.9433 | 0.2075 | 10.6752 | 100.225 |
| 2764.9 | 2.4428 | 8.1853 | 49.3523 | 0.2101 | 11.697 | 101.251 |
| 2765 | 2.42602 | 8.182 | 49.431 | 0.2161 | 12.7418 | 102.238 |
| 2765.1 | 2.40865 | 8.18 | 48.7863 | 0.2203 | 14.1103 | 103.397 |
| 2765.2 | 2.38987 | 8.179 | 47.288 | 0.2238 | 15.7359 | 104.593 |
| 2765.3 | 2.36979 | 8.179 | 44.936 | 0.2266 | 17.5222 | 105.828 |
| 2765.4 | 2.35375 | 8.1817 | 42.1407 | 0.225 | 19.6311 | 106.803 |
| 2765.5 | 2.34244 | 8.185 | 40.0613 | 0.2216 | 22.0109 | 107.557 |
| 2765.6 | 2.33574 | 8.189 | 38.698 | 0.2164 | 24.6603 | 108.091 |
| 2765.7 | 2.33576 | 8.1917 | 39.1053 | 0.2184 | 28.0487 | 108.316 |
| 2765.8 | 2.33647 | 8.193 | 40.0173 | 0.2225 | 31.5392 | 108.489 |
| 2765.9 | 2.33778 | 8.193 | 41.434 | 0.2287 | 34.9493 | 108.609 |
| 2766 | 2.33707 | 8.193 | 43.008 | 0.2337 | 37.4216 | 108.637 |
| 2766.1 | 2.33477 | 8.1933 | 44.0723 | 0.2376 | 39.5032 | 108.612 |
| 2766.2 | 2.33075 | 8.194 | 44.627 | 0.2402 | 41.1345 | 108.534 |
| 2766.3 | 2.32202 | 8.1933 | 43.0197 | 0.2435 | 42.4011 | 108.489 |
| 2766.4 | 2.31237 | 8.192 | 40.5277 | 0.2469 | 44.2208 | 108.577 |
| 2766.5 | 2.30162 | 8.19 | 37.151 | 0.2504 | 46.4597 | 108.798 |
| 2766.6 | 2.29359 | 8.19 | 34.131 | 0.2456 | 51.8172 | 109.361 |
| 2766.7 | 2.28827 | 8.191 | 31.952 | 0.2398 | 59.0138 | 109.98 |
| 2766.8 | 2.28557 | 8.193 | 30.614 | 0.2331 | 67.6841 | 110.654 |
| 2766.9 | 2.28156 | 8.1937 | 30.29 | 0.2308 | 76.3316 | 111.154 |
| 2767 | 2.27484 | 8.1943 | 29.8013 | 0.229 | 82.3606 | 111.57 |
| 2767.1 | 2.27023 | 8.1947 | 29.4747 | 0.2283 | 83.9932 | 111.736 |
| 2767.2 | 2.26049 | 8.1957 | 28.674 | 0.2283 | 84.2625 | 112.085 |
| 2767.3 | 2.25046 | 8.197 | 27.726 | 0.2296 | 81.5197 | 112.452 |
| 2767.4 | 2.24645 | 8.197 | 26.9173 | 0.2334 | 77.0781 | 112.88 |

Table 7 is a well log for 3 meter vertical section. First column is showing depth and log data values are available per 0.1 meters. Based on these available log data petrophysical parameters and lithology identification have been performed for 0.1 meter increment.

However, in Pereriv D C01 well is completely absent for this study. Moreover, GCA4 well has no density log for Pereriv D section.

Conventional cores have also been taken from some of the wells in order to integrate well log with core plug data to have a reliable reservoir description. Among nine wells mentioned above only 7 of them have core data. These data set includes permeability of air, pore throat size, calculated microporosity including fractures, calculated microporosity excluding fractures, HG porosity, 400 PSI porosity and permeability. Table 8 is an example which includes all of these data for GCA 1 well.

**Table 8.** Core data for GCA1 well

| Depth (dd, RKB, m) | Total Macroporosity (excl.Fracture) | $K_{air}$ (mD) | $r_{35}$ | k/phi | Calculated Microporosity | Hg Porosity (%) | 400 PSI Porosity (%) |
|---|---|---|---|---|---|---|---|
| 2664.32 | 5.2 | 0 | 0.1 | 0 | 10.2 | 13 | 10.1 |
| 2671.09 | 4.2 | 11.36 | 1.79 | 2.6 | 17.1 | 22 | 20.8 |
| 2682.39 | 0 | 860.08 | 6.37 | | 10.5 | 27.6 | 27.4 |
| 2685.34 | 11.5 | 82.69 | 0 | 7.2 | 16.91 | 10 | 16.9 |
| 2687.33 | 9.1 | 508.1 | 2.98 | 55.9 | 14.8 | 19.7 | 21.3 |
| 2698.31 | 4.3 | 0.33 | 0.32 | 0.1 | 6 | 14 | 6.1 |
| 2708.31 | 0.5 | 163.84 | 5.87 | 327.7 | 12.5 | 25.8 | 23.9 |
| 2710.43 | 16.5 | 109.9 | 3.25 | 6.7 | 15.9 | 22.4 | 21.1 |
| 2770.43 | 0 | 236.03 | 5.87 | | 13.5 | 24.5 | 23.1 |
| 2775.33 | 9.5 | 37.1 | 2.53 | 3.9 | 8.8 | 21.9 | 20.8 |
| 2780.56 | 3.8 | 520.7 | 0 | 134.9 | 7.2 | 28 | 25.5 |
| 2785.1 | 7.7 | 919.5 | 27.8 | 118.3 | 2.7 | 31.8 | 24.1 |
| 2788.35 | 17 | 20.38 | 3.85 | 1.2 | 8.4 | 16.1 | 23.3 |
| 2792.3 | trace | 11.55 | 2.12 | | 8.4 | 17.4 | 14.5 |
| 2798.35 | 5.6 | 487.99 | 18.6 | 86.1 | 9.4 | 33.2 | 23.9 |
| 2803.3 | trace | 121.17 | 4.19 | | 11.4 | 22 | 21.7 |
| 2808.52 | 3.3 | 318.96 | 8.18 | 94.1 | 5.5 | 21.4 | 22.2 |
| 2819.36 | 11.1 | 184.83 | 5.39 | 16.6 | 9.7 | 25.2 | 22.1 |
| 2823.31 | 5.2 | 147.3 | 5.39 | 28.2 | 14.5 | 26.6 | 24.1 |
| 2829.63 | 8.6 | 0 | 8.18 | 0 | nm | 25 | |
| 2833.61 | 11.5 | 119.37 | 2.3 | 10.4 | 17.8 | 22.7 | 26.4 |
| 2838.34 | 16 | 0.47 | 0.54 | 0.1 | 11.6 | | 15.1 |
| 2848.36 | 18.1 | 17.05 | 0.42 | 1 | 10.9 | 14.8 | 11.4 |

Because of the problems and difficulties of core taking, scale of the core examples are inconsistent. In some points even some of the parameters were not able to estimate.

### 5.2 Histogram Analysis

Histograms are used to simply show the distribution of a quantitative variable by its relative frequency of data points in an interval. The histogram function in SPSS gives the option of overlaying a normal curve. If there is a strong deviation from the normal distribution or if the distribution mean is off-set far from 0, then this might tell you something about possible problems with the data (e.g. measurement or calculation errors might lead to a non-normal distribution) or also show severe nutrition problems in the population. Histograms are most useful for continuous data to see if the distribution is normal and whether there is adequate data cleaning. Also, histograms are useful for determining arbitrary cut-points for creating categories from continuous

data. By using SPSS, porosity (core and density porosity) histogram plots have been plotted for Pereriv B and Pereriv D. Main aim was to compare core and log porosities.

Figure 12 is a histogram chart of GCA1 well. The wells have both core and well log porosities. And the vertical interval selected to construct histogram chart was the same as the core interval.

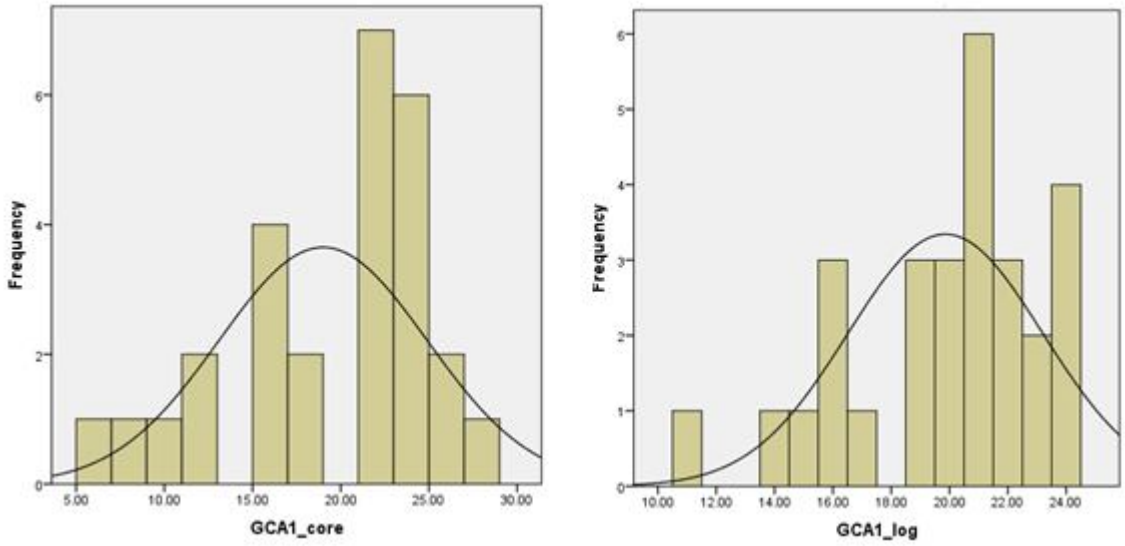


**Figure 13.**Histogram chart of porosity from well log and core in GCA1 well

Figure 13 shows that there is some similarity between core and log porosity in GCA1 well. Because of lack data in the core analysis it is not very identical.

Figure 14 is another example of GCA4 well's core and log porosity histogram chart. Generally small interval was cored and that interval was selected for this analysis. Therefore, almost in all charts histograms do not fit to normal curve.

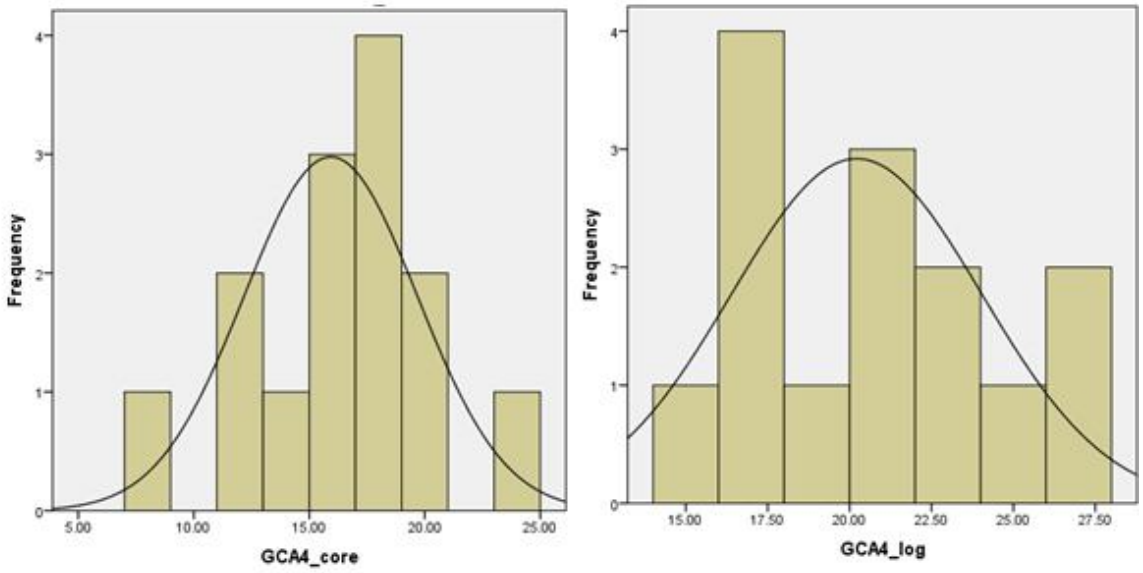


**Figure 14.**Histogram chart of porosity from well log and core in GCA4 well

Figure 14 shows two different porosity distributions. Log porosity distribution is slightly negatively skewed. Unlike it core porosity is normal distributed but there are still some gaps which make it to be unfit to normal curve.

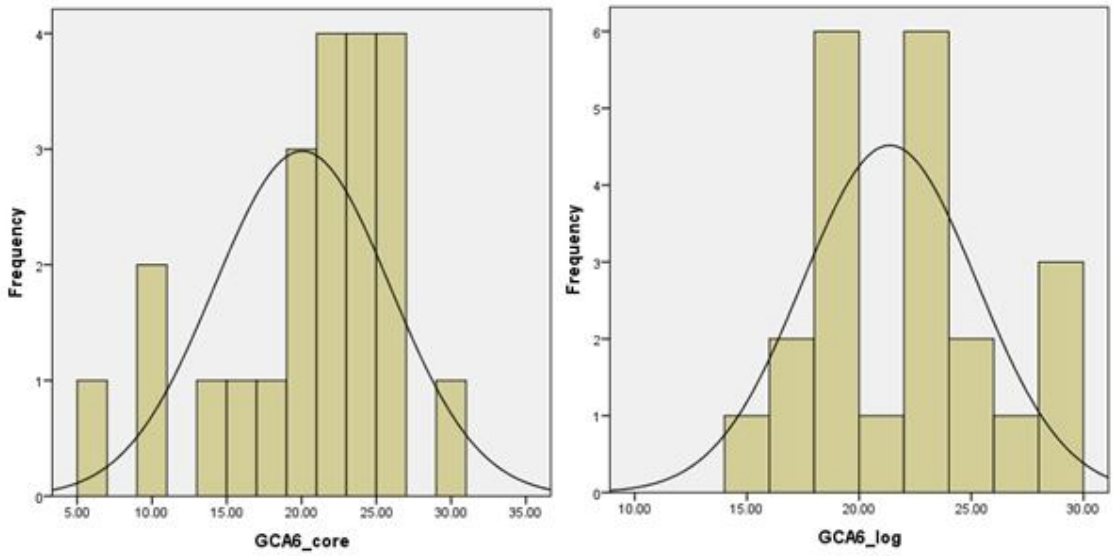


**Figure 15.**Histogram chart of porosity from well log and core in GCA6 well.

In GCA6 core and well log porosity distribution is also different. It may be explained by the insufficient data. However, normal curves for GCA6 well are the same.

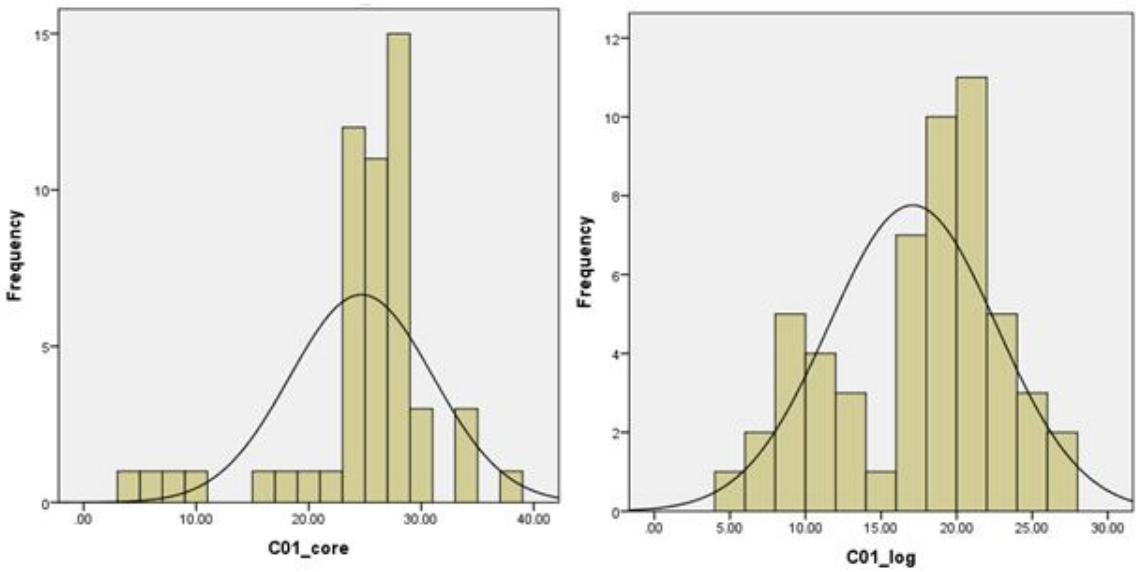


**Figure 16.**Histogram chart of porosity from well log and core in C01 well.

Figure 16 is another example of comparison of histogram charts for C01. As it can be noticed in the figure core porosity is not enough to make clear similarities. On the other hand pattern of the normal curve frequencies is slightly identical.

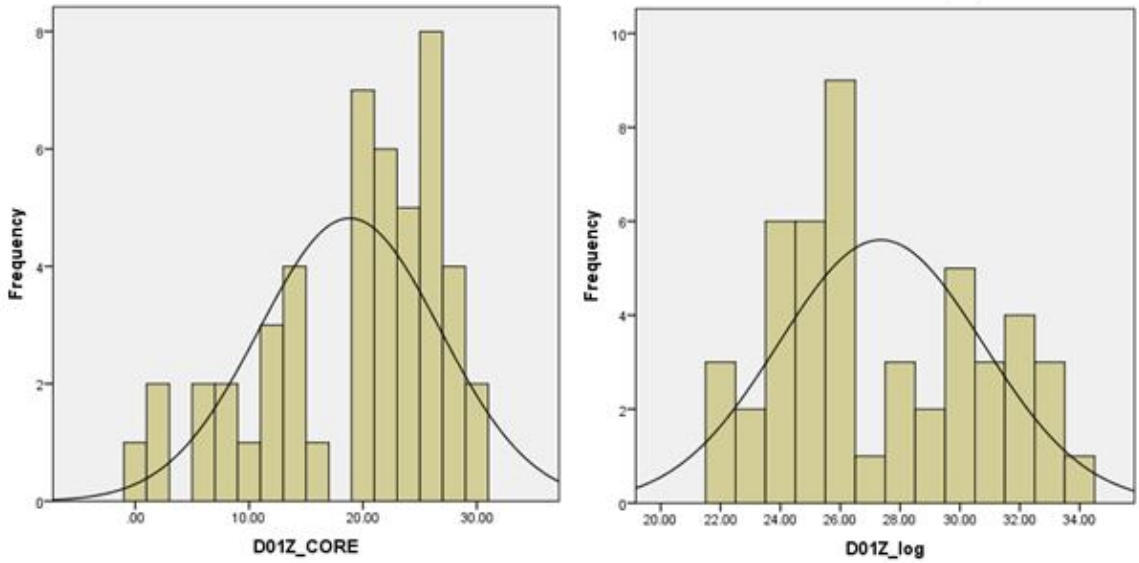


**Figure 17.** Histogram chart of porosity from well log and core in D01Z well.

In last example (Figure 17) log porosity does not fit to normal curve distribution. However, small porosity values in core example fit to normal curve.

Furthermore, it was mentioned in previous chapter that in Pereriv D there was no core data for this study. Therefore, well logs have been used in characterization of the reservoir. Also same histogram analysis was performed on Pereriv D based on well log data. The similar results have been obtained. Moreover, frequencies of density porosities of both formations have been compared by correlation coefficient and it was realized that they are related. Table 9 is frequency table of density porosity for Pereriv B and D. And again SPSS has been used in calculation of density log porosity frequencies.

**Table 9.** Correlation coefficients between Pereriv B and D in A08Z and GCA6

| A08Z | | |
|---|---|---|
| Porosity | Fre_PerB | Fre_PerD |
| 0 | 1 | 1 |
| 1 | 3 | 2 |
| 2 | 8 | 2 |
| 3 | 10 | 3 |
| 4 | 8 | 12 |
| 5 | 12 | 19 |
| 6 | 16 | 32 |
| 7 | 13 | 24 |
| 8 | 21 | 21 |
| 9 | 16 | 25 |
| 10 | 28 | 34 |
| 11 | 37 | 31 |
| 12 | 54 | 26 |
| 13 | 52 | 31 |
| 14 | 67 | 25 |
| 15 | 67 | 18 |
| 16 | 57 | 23 |
| 17 | 54 | 14 |
| 18 | 60 | 14 |
| 19 | 50 | 6 |
| 20 | 33 | 0 |
| 21 | 43 | 0 |
| 22 | 24 | 0 |
| 23 | 4 | 0 |
| | Corr coef | 0.428297 |

| GCA6 | | |
|---|---|---|
| Porosity | Fre_PerB | Fre_PerD |
| 2 | 0 | 1 |
| 3 | 0 | 1 |
| 4 | 0 | 1 |
| 5 | 0 | 0 |
| 6 | 0 | 4 |
| 7 | 2 | 2 |
| 8 | 2 | 5 |
| 9 | 2 | 3 |
| 10 | 5 | 2 |
| 11 | 2 | 1 |
| 12 | 6 | 3 |
| 13 | 4 | 9 |
| 14 | 8 | 10 |
| 15 | 21 | 10 |
| 16 | 16 | 18 |
| 17 | 33 | 26 |
| 18 | 36 | 19 |
| 19 | 54 | 15 |
| 20 | 58 | 6 |
| 21 | 23 | 2 |
| 22 | 15 | 0 |
| 23 | 7 | 0 |
| 24 | 1 | 0 |
| | Corr coef | 0.598039 |

In Table 9 correlation coefficients of Pereriv B and Pereriv D are 0.42 and 0.59 which is not very high. Here it is worthy to mention that In Pereriv B the vertical section which is chosen for correlation with Pereriv D corresponds to flow unit. Therefore similarity of these two sections can mean possible flow unit in Pereriv D. In Table 10 the same correlation of Pereriv B and Pereriv D is shown for another well.

**Table 10.** Correlation coefficient between Pereriv B and D in B01ST1

| B01ST1 | | |
|---|---|---|
| Porosity | Fre_PerB | Fre_PerD |
| 8 | 3 | 0 |
| 9 | 4 | 0 |
| 10 | 2 | 5 |
| 11 | 2 | 5 |
| 12 | 1 | 4 |
| 13 | 1 | 1 |
| 14 | 2 | 4 |
| 15 | 1 | 10 |
| 16 | 5 | 5 |
| 17 | 3 | 6 |
| 18 | 4 | 9 |
| 19 | 9 | 8 |
| 20 | 10 | 13 |
| 21 | 14 | 20 |
| 22 | 14 | 14 |
| 23 | 29 | 20 |
| 24 | 13 | 31 |
| 25 | 38 | 44 |
| 26 | 34 | 44 |
| 27 | 52 | 15 |
| 28 | 41 | 12 |
| 29 | 40 | 0 |
| 30 | 34 | 0 |
| 31 | 53 | 0 |
| 32 | 24 | 0 |
| 33 | 17 | 0 |
| 34 | 5 | 0 |
| | Corr coef | 0.30444072 |

Again B01ST1 well shows low correlation coefficient meaning that the two formations in B01ST1 well are not related to each other. However, in next tables correlation coefficients of Pereriv B and Pereriv D in GCA1, GCA2, and D01Z wells are high enough. In GCA1 well it is 0.89 which can be considered very good correlation between Pereriv B and Pereriv D. Therefore, it can be concluded that in this two formations porosity is controlling by the same parameters which is very similar. On the other hand in GCA2 well correlation coefficient of Pereriv B and Pereriv D based on porosity value 0.85 which is slightly lower than GCA1 well but still it is high enough to consider it identical.

As shown in Table 11 D01Z well has also high correlation coefficient 0.81. Generally last three wells mentioned in Table 11 has the highest correlation coefficients among other wells.

**Table 11.** Correlation coefficients between Pereriv B and D in GCA1, GCA2 and D01Z

| GCA1 | | |
|---|---|---|
| Porosity | Fre_PerB | Fre_PerD |
| 9 | 5 | 0 |
| 10 | 4 | 4 |
| 11 | 3 | 6 |
| 12 | 5 | 5 |
| 13 | 5 | 3 |
| 14 | 11 | 3 |
| 15 | 12 | 13 |
| 16 | 23 | 27 |
| 17 | 47 | 27 |
| 18 | 53 | 30 |
| 19 | 90 | 60 |
| 20 | 89 | 43 |
| 21 | 45 | 53 |
| 22 | 5 | 16 |
| | Corr coef | 0.892644 |

| GCA2 | | |
|---|---|---|
| Porosity | Fre_PerB | Fre_PerD |
| 12 | 1 | 3 |
| 13 | 8 | 4 |
| 14 | 8 | 3 |
| 15 | 8 | 8 |
| 16 | 14 | 6 |
| 17 | 14 | 4 |
| 18 | 26 | 9 |
| 19 | 31 | 7 |
| 20 | 51 | 6 |
| 21 | 66 | 8 |
| 22 | 93 | 31 |
| 23 | 94 | 53 |
| 24 | 91 | 45 |
| 25 | 39 | 35 |
| 26 | 6 | 8 |
| 28 | 3 | 0 |
| 30 | 3 | 0 |
| 31 | 4 | 0 |
| 32 | 2 | 0 |
| 34 | 1 | 0 |
| 35 | 1 | 0 |
| 36 | 1 | 0 |
| | Corr coef | 0.853768 |

| D01Z | | |
|---|---|---|
| Porosity | Fre_PerB | Fre_PerD |
| 13 | 1 | 0 |
| 15 | 3 | 0 |
| 16 | 2 | 0 |
| 17 | 5 | 2 |
| 18 | 6 | 2 |
| 19 | 4 | 1 |
| 20 | 7 | 2 |
| 21 | 10 | 6 |
| 22 | 17 | 6 |
| 23 | 27 | 14 |
| 24 | 20 | 1 |
| 25 | 5 | 2 |
| 26 | 3 | 0 |
| 27 | 4 | 0 |
| | Corr coef | 0.815897 |

Moreover, GCA5 is another well which has also high correlation between Pereriv B and Pereriv D. Table 12 is a frequency table showing this correlation. In this table we have 22 porosity values which are encountered both in Pereriv B and Pereriv D. And correlation coefficient between them is 0.71.

**Table 12.** Correlation coefficients between Pereriv B and D in GCA5 well

| GCA5 | | |
|---|---|---|
| Porosity | Fre_PerB | Fre_PerD |
| 5 | 1 | 0 |
| 6 | 2 | 3 |
| 7 | 1 | 5 |
| 8 | 2 | 8 |
| 9 | 6 | 5 |
| 10 | 22 | 6 |
| 11 | 14 | 6 |
| 12 | 14 | 8 |
| 13 | 15 | 6 |
| 14 | 10 | 19 |
| 15 | 13 | 28 |
| 16 | 21 | 10 |
| 17 | 34 | 25 |
| 18 | 34 | 19 |
| 19 | 42 | 29 |
| 20 | 74 | 52 |
| 21 | 71 | 47 |
| 22 | 66 | 38 |
| 23 | 54 | 7 |
| 24 | 53 | 0 |
| 25 | 30 | 0 |
| 26 | 2 | 0 |
| | Corr coef | 0.707077 |

Based on the histogram analysis these tables have been constructed and correlation coefficients have been found between Pereriv B and Pereriv D. And the vertical section for this study chosen in Pereriv B was flow zone and therefore, high correlation coefficient may indicate flow unit zonation in Pereriv D. Except A08Z and B01ST1 wells other wells showed high correlation.

### 5.2 Principal Component Analysis

Principal Component Analysis or simply PCA is considered for the relationship of the variables in the data matrix. In a geometrical point of view, relationship of two variables can be illustrated in x-y plot of Figure 18 where a marked tendency can be noticed for big values of x to be related to big values of y. If x and y are standardized variables, this tendency may be measured by the mean value of the product $x \bullet y$ of the standardized values. As before to get away from the errors or for desk calculator use, the value is estimated from the raw data, and a more complex equation is used, in which the covariance, or average cross-product of the deviations from the means of the two variables,, is divided by the product of their standard deviations. The result, in either case, is the correlation coefficient between x and y, for which the symbol r is often used. With one correlation coefficient between each pair of the variables, a data matrix of n variates gives rise to an n x n matrix of correlation coefficient, sometimes termed the matrix. Because the

correlation between x and y is the same as that between y and x, the r matrix has the same values above and below the main diagonal.

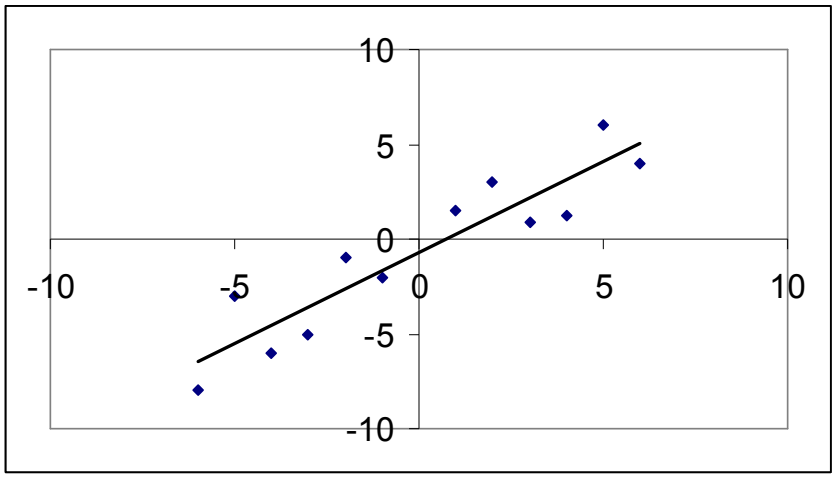


**Figure 18**. x and y plot of distribution

The main idea of this method is to form, from a set of existing variables, a new variable (or new variables, but as few as possible) that contain as much variability of the original data as possible. This is a method of data reduction; we reduce the number of variables in order to handle data more easily. In most cases we wish to get only one dimension (variable) that contains most of the variability of the original data. This variable represents some sort of index of a certain property that is measured by the original variables.

Principal components analysis is a method of data reduction. Suppose that you have a dozen variables that are correlated. You might use principal components analysis to reduce your 12 measures to a few principal components. In this example, you may be most interested in obtaining the component scores (which are variables that are added to your data set) and/or to look at the dimensionality of the data. For example, if two components are extracted and those two components accounted for 68% of the total variance, then we would say that two dimensions in the component space account for 68% of the variance. Principal components analysis, like factor analysis, can be performed on raw data, as shown in this example, or on a correlation or a covariance matrix. If raw data are used, the procedure will create the original correlation matrix or covariance matrix, as specified by the user. If the correlation matrix is used, the variables are standardized and the total variance will equal the number of variables used in the analysis (because each standardized variable has a variance equal to 1). If the covariance matrix is used, the variables will remain in their original metric. However, one must take care to use variables whose variances and scales are similar.

There are several softwares that can utilize PCA. In our research SPSS have been used and many options were included. All 9 wells of Pereriv B and Pereriv D and their density porosity values are used as an input for SPSS and the results are shown below.

Table 13 is output because we used the univariate option. Also note that the values shown in the table are the mean, standard deviation and sample size of porosity which has been derived from porosity logging

**Table 13.** Descriptive statistics of density porosity for the wells

**Descriptive Statistics**

| Wells | Mean | Std. Deviation | Analysis N |
|---|---|---|---|
| GCA1 | 38.5 | 3.5 | 113 |
| GCA2 | 29.5 | 1.1 | 113 |
| GCA4 | 23.7 | 1.2 | 113 |
| GCA5 | 32.1 | 2.9 | 113 |
| GCA6 | 24.5 | 2.4 | 113 |
| C01 | 28.3 | 5.9 | 113 |
| D01Z | 30.7 | 1.9 | 113 |
| B01ST1 | 40.1 | 2.6 | 113 |
| A08Z | 17.5 | 2.4 | 113 |

Table 14 is a correlation table showing the correlations between the original variables

**Table 14.** Correlation matrix of the components

**Correlation Matrix**

| | | GCA1 | GCA2 | GCA4 | GCA5 | GCA6 | C01 | D01Z |
|---|---|---|---|---|---|---|---|---|
| Correlation | GCA1 | 1.000 | .385 | -.221 | .398 | -.146 | .105 | .195 |
| | GCA2 | .385 | 1.000 | -.072 | .246 | -.232 | .003 | .271 |
| | GCA4 | -.221 | -.072 | 1.000 | .006 | -.028 | .467 | -.133 |
| | GCA5 | .398 | .246 | .006 | 1.000 | -.182 | .264 | .114 |
| | GCA6 | -.146 | -.232 | -.028 | -.182 | 1.000 | -.070 | -.037 |
| | C01 | .105 | .003 | .467 | .264 | -.070 | 1.000 | -.111 |
| | D01Z | .195 | .271 | -.133 | .114 | -.037 | -.111 | 1.000 |
| | B01ST1 | .104 | .023 | -.038 | -.030 | -.081 | .041 | -.037 |
| | A08Z | -.188 | .070 | -.289 | -.191 | .036 | -.458 | .140 |
| Sig. (1-tailed) | GCA1 | | .000 | .009 | .000 | .062 | .133 | .019 |
| | GCA2 | .000 | | .223 | .004 | .007 | .486 | .002 |
| | GCA4 | .009 | .223 | | .473 | .384 | .000 | .079 |
| | GCA5 | .000 | .004 | .473 | | .027 | .002 | .115 |
| | GCA6 | .062 | .007 | .384 | .027 | | .230 | .348 |
| | C01 | .133 | .486 | .000 | .002 | .230 | | .120 |
| | D01Z | .019 | .002 | .079 | .115 | .348 | .120 | |
| | B01ST1 | .137 | .404 | .344 | .375 | .198 | .332 | .347 |
| | A08Z | .023 | .232 | .001 | .021 | .353 | .000 | .070 |

Table 15 shows Kaiser-Meyer-Olkin Measure of Sampling Adequacy and Bartlett's Test of Sphericity - This measure varies between 0 and 1, and values closer to 1 are better.

**Table 15**. KMO and Bartlett's Test

**KMO and Bartlett's Test**

| | | |
|---|---|---|
| Kaiser-Meyer-Olkin Measure of Sampling Adequacy. | | .629 |
| Bartlett's Test of Sphericity | Approx. Chi-Square | 143.331 |
| | df | 36 |
| | Sig. | .000 |

Bartlett's Test of Sphericity tests the null hypothesis that the correlation matrix is an identity matrix. An identity matrix is matrix in which all of the diagonal elements are 1 and all off diagonal elements are 0. You want to reject this null hypothesis. Taken together, these tests provide a minimum standard which should be passed before a principal components analysis (or a factor analysis) should be conducted.

**Table 16.**Communalities

**Communalities**

| | Initial | Extraction |
|---|---|---|
| GCA1 | 1.000 | .633 |
| GCA2 | 1.000 | .531 |
| GCA4 | 1.000 | .633 |
| GCA5 | 1.000 | .531 |
| GCA6 | 1.000 | .196 |
| C01 | 1.000 | .714 |
| D01Z | 1.000 | .406 |
| B01ST1 | 1.000 | .778 |
| A08Z | 1.000 | .606 |

Communalities - This is the proportion of each variable's variance that can be explained by the principal components. Initial - By definition, the initial value of the communality in principal components analysis is 1. Extraction - The values in this column indicate the proportion of each variable's variance that can be explained by the principal components. Variables with high values are well represented in the common factor space, while variables with low values are not well represented. They are the reproduced variances from the number of components that you have saved. You can find these values on the diagonal of the reproduced correlation matrix.

**Table 17.** Total Variance Explained

**Total Variance Explained**

| Component | Initial Eigenvalues | | | Extraction Sums of Squared Loadings | | |
|---|---|---|---|---|---|---|
| | Total | % of Variance | Cumulative % | Total | % of Variance | Cumulative % |
| 1 | 2.052 | 22.801 | 22.801 | 2.052 | 22.801 | 22.801 |
| 2 | 1.896 | 21.063 | 43.864 | 1.896 | 21.063 | 43.864 |
| 3 | 1.081 | 12.013 | 55.878 | 1.081 | 12.013 | 55.878 |
| 4 | .968 | 10.758 | 66.635 | | | |
| 5 | .861 | 9.571 | 76.207 | | | |
| 6 | .669 | 7.429 | 83.636 | | | |
| 7 | .608 | 6.754 | 90.390 | | | |
| 8 | .457 | 5.079 | 95.468 | | | |
| 9 | .408 | 4.532 | 100.000 | | | |

In Table 17 several options have been illustrated. Component - There are as many components extracted during a principal components analysis as there are variables that are put into it. In our example, we used 9 variables so we have 9 components. InitialEigenvalues - Eigenvalues are the variances of the principal components. Because we conducted our principal components analysis on the correlation matrix, the variables are standardized, which means that the each variable has a variance of 1, and the total variance is equal to the number of variables used in the analysis, in this case, 9. Total - This column contains the eigenvalues. The first component will always account for the most variance (and hence have the highest eigenvalue), and the next component will account for as much of the left over variance as it can, and so on. Hence, each successive component will account for less and less variance. % of Variance - This column contains the percent of variance accounted for by each principal component. Cumulative % - This column contains the cumulative percentage of variance accounted for by the current and all preceding principal components. For example, the third row shows a value of 68.313. This means that the first three components together account for 55.878% of the total variance. Cumulative % - This column contains the cumulative percentage of variance accounted for by the current and all preceding principal components. For example, the third row shows a value of 68.313. This means that the first three components together account for 68.313% of the total variance.

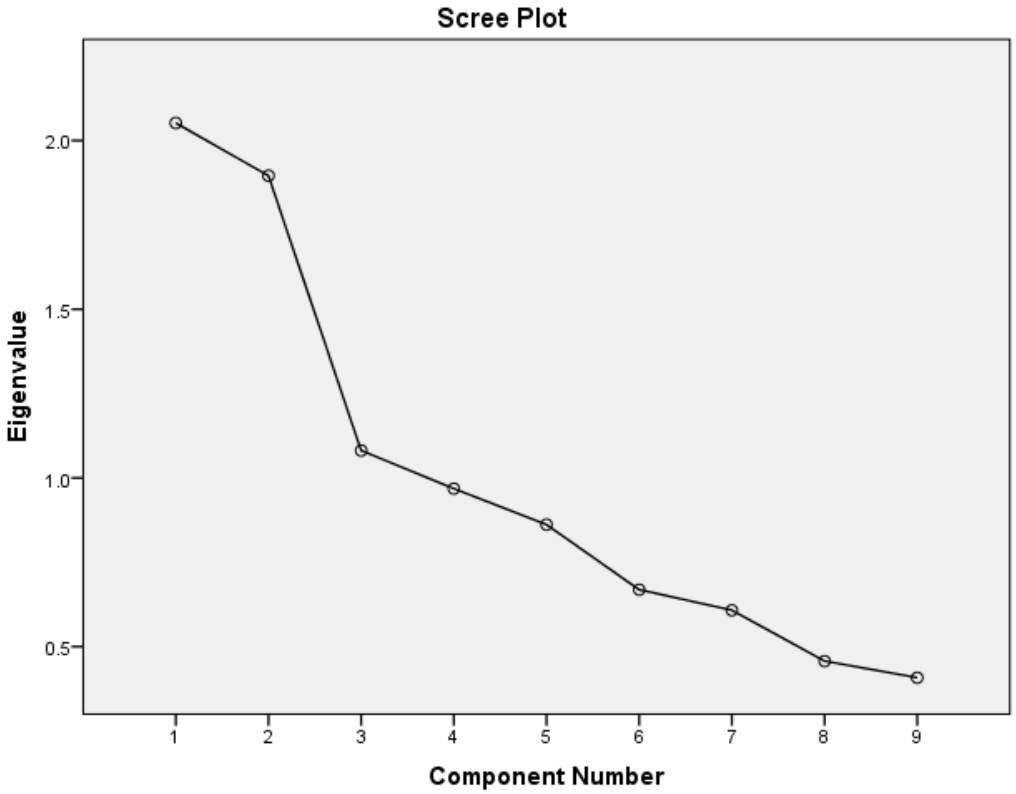


**Figure 19.** Scree plot of principal components

The scree plot (Figure 18) graphs the eigenvalue against the component number. You can see these values in the first two columns of the table immediately above. From the third component on, you can see that the line is almost flat, meaning the each successive component is accounting for smaller and smaller amounts of the total variance. In general, we are interested in keeping only those principal components whose eigenvalues are greater than 1. Components with an eigenvalue of less than 1 account for less variance than did the original variable (which had a variance of 1), and so are of little use. Hence, you can see that the point of principal components analysis is to redistribute the variance in the correlation matrix (using the method of eigenvalue decomposition) to redistribute the variance to first components extracted.

**Table 18.** Component matrix

**Component Matrix**

| | Component | | |
|---|---|---|---|
| | 1 | 2 | 3 |
| GCA5 | .690 | .157 | .174 |
| GCA1 | .646 | .435 | -.164 |
| C01 | .600 | -.579 | .138 |
| A08Z | -.549 | .516 | .196 |
| GCA6 | -.398 | -.173 | .089 |
| GCA4 | .238 | -.691 | .315 |
| D01Z | .159 | .539 | .300 |
| GCA2 | .479 | .531 | .139 |
| B01ST1 | .165 | -.023 | -.866 |

Component Matrix - This table contains component loadings, which are the correlations between the variable and the component. Because these are correlations, possible values range from -1 to +1. On the /format subcommand, we used the option blank (.30), which tells SPSS not to print any of the correlations that are .3 or less. This makes the output easier to read by removing the clutter of low correlations that are probably not meaningful anyway. Component - The columns under this heading are the principal components that have been extracted. As you can see by the footnote provided by SPSS, three components were extracted (the two components that had an eigenvalue greater than 1). You usually do not try to interpret the components the way that you would factors analysis that have been extracted from a factor analysis. Rather, most people are interested in the component scores, which are used for data reduction (as opposed to factor analysis where you are looking for underlying latent continua). You can save the component scores to your data set for use in other analyses using the /save subcommand.

Table 19 contains two tables, the reproduced correlations in the top part of the table, and the residuals in the bottom part of the table. Reproduced Correlation - The reproduced correlation matrix is the correlation matrix based on the extracted components. You want the values in the reproduced matrix to be as close to the values in the original correlation matrix as possible. This means that you want the residual matrix, which contains the differences between the original and the reproduced matrix, to be close to zero.

**Table 19.** Reproduced correlations of principal components

**Reproduced Correlations**

| | | GCA1 | GCA2 | GCA4 | GCA5 | GCA6 | C01 |
|---|---|---|---|---|---|---|---|
| Reproduced Correlation | GCA1 | .633[a] | .518 | -.199 | .486 | -.347 | .113 |
| | GCA2 | .518 | .531[a] | -.209 | .438 | -.270 | -.001 |
| | GCA4 | -.199 | -.209 | .633[a] | .110 | .053 | .586 |
| | GCA5 | .486 | .438 | .110 | .531[a] | -.286 | .347 |
| | GCA6 | -.347 | -.270 | .053 | -.286 | .196[a] | -.126 |
| | C01 | .113 | -.001 | .586 | .347 | -.126 | .714[a] |
| | D01Z | .288 | .404 | -.240 | .247 | -.130 | -.175 |
| | B01ST1 | .239 | -.054 | -.218 | -.040 | -.138 | -.007 |
| | A08Z | -.163 | .038 | -.426 | -.264 | .147 | -.601 |
| Residual | GCA1 | | -.133 | -.022 | -.088 | .201 | -.008 |
| | GCA2 | -.133 | | .137 | -.192 | .038 | .004 |
| | GCA4 | -.022 | .137 | | -.103 | -.081 | -.119 |
| | GCA5 | -.088 | -.192 | -.103 | | .104 | -.082 |
| | GCA6 | .201 | .038 | -.081 | .104 | | .056 |
| | C01 | -.008 | .004 | -.119 | -.082 | .056 | |
| | D01Z | -.093 | -.134 | .107 | -.133 | .093 | .063 |
| | B01ST1 | -.135 | .077 | .179 | .010 | .058 | .048 |
| | A08Z | -.026 | .032 | .136 | .072 | -.111 | .144 |

If the reproduced matrix is very similar to the original correlation matrix, then you know that the components that were extracted accounted for a great deal of the variance in the original correlation matrix, and these few components do a good job of representing the original data. The numbers on the diagonal of the reproduced correlation matrix are presented in the Communalities table in the column labeled Extracted. Residual - As noted in the first footnote provided by SPSS (a.), the values in this part of the table represent the differences between original correlations (shown in the correlation table at the beginning of the output) and the reproduced correlations, which are shown in the top part of this table.

# CHAPTER 6

# RESULTS AND DISCUSSIONS

As it is already mentioned that the sedimentary environment in the region was fluvio-deltaic which lead deposition of clastic sediments. Therefore, usually we see sandstone and shale alteration in the wells which have been drilled. From the core data it is obtained that Pereriv B consists of sandstone and thin shale beddings. Moreover, from the GR log Vshale has been estimated. And the result is plotted versus depth. Figure 20 shows the volume of shale in all 9 wells drilled to Pereriv B. In the figure wells are aligned from NW to SE

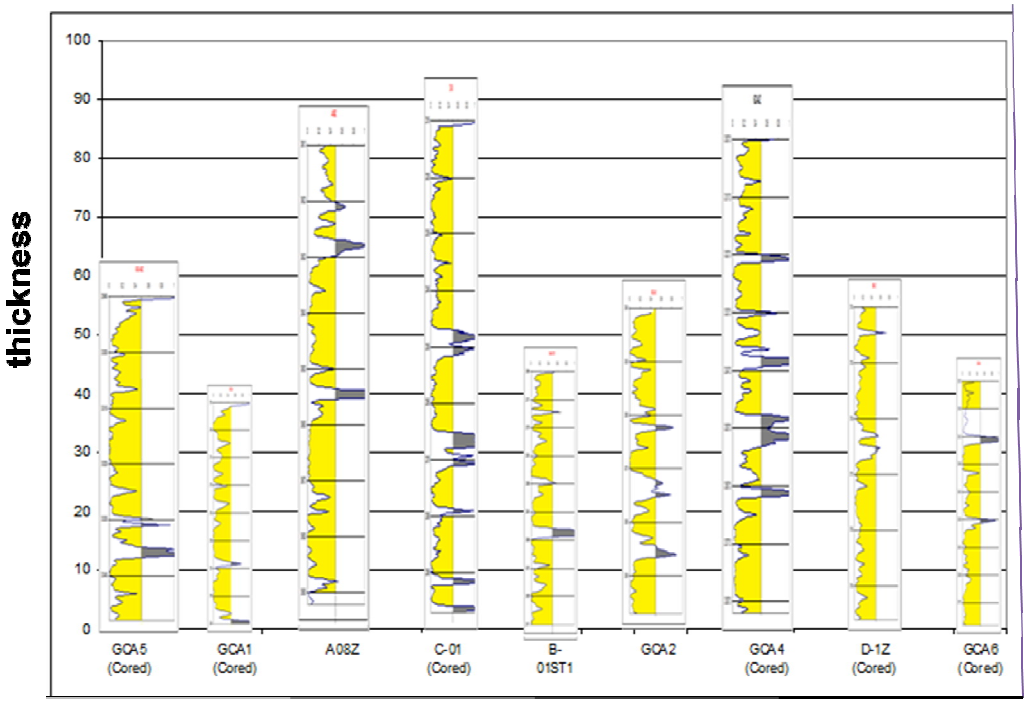


**Figure 20.** Volume of shale versus depth. Yellow parts indicates clean sandstone, grey parts indicates shale

As mentioned in previous chapters, 9 wells are available for this study. In all 9 wells well logs have been run and some of them have been cored. The interpretation of well log, core data and summary of statistical analysis shows that there is a separation in Pereiv B formation. This separation was observed by the dramatically increase in permeability and pore throat size Moreover, porosity value is also getting high in this zone. Figure 20 is one example of showing

this separation. Upper part of the section exhibit distinct pattern and indicates our determined flow unit. Therefore, it can be thought that this zone of same flow characteristics can comprise same flow unit. Also, this zone which is characterized by the high porosity, permeability and pore throat size are observable in all wells.

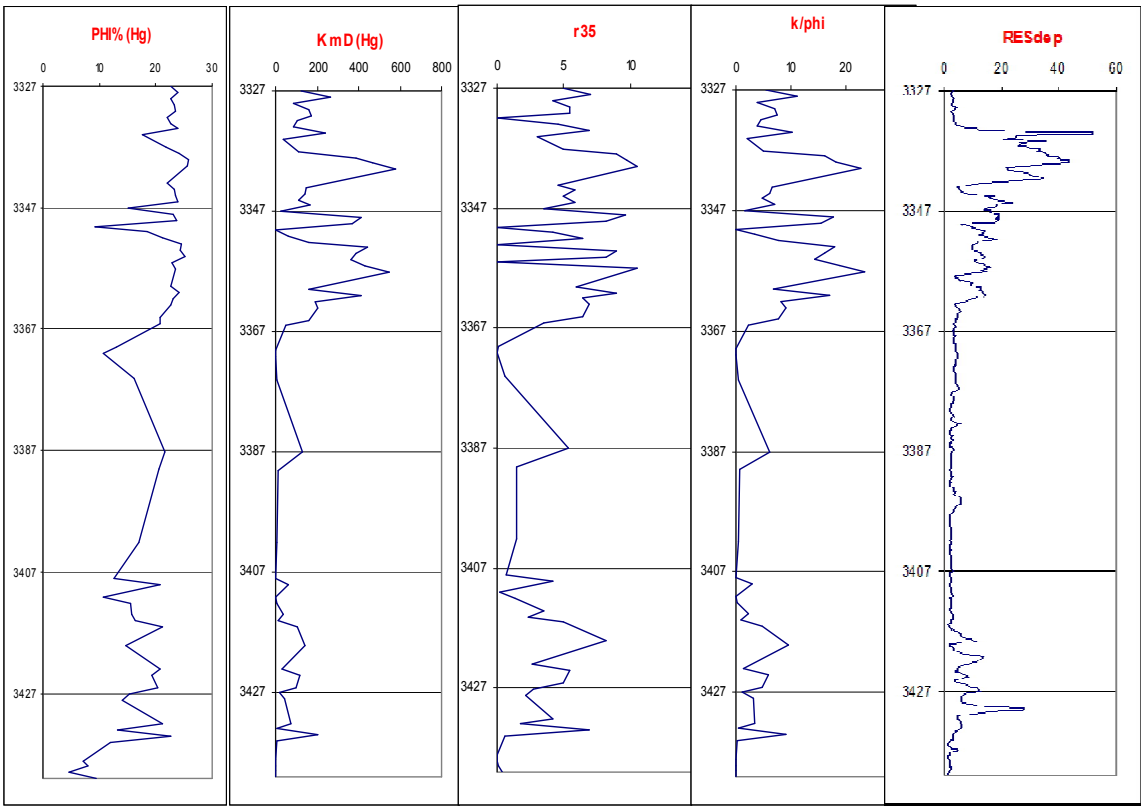


**Figure 21.** Porosity permeability, ratio of them and r35 values with depth. Well GCA6, Pereriv B

The core plug analysis, port-size study, and the k/Ø analysis showed that the data samples clustered around this unit.

Furthermore, statistical methods have been also utilized to find a relationship between Pereriv B and Pereriv D. First of all histogram analysis has been applied and porosity frequency plots have been constructed. General tendency of the porosity histograms are very close to normal distribution. Figure 21 is an example of histogram chart of A08Z which is very similar to normal distribution.

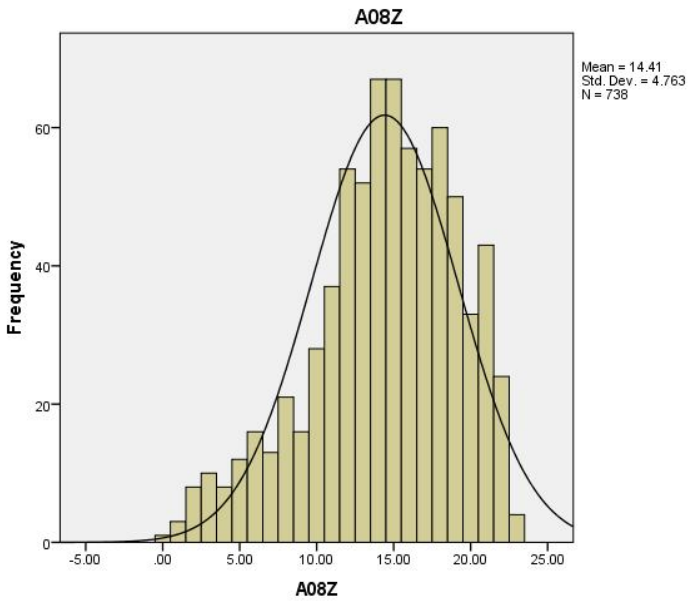


**Figure 22.**Histogram chart of porosity. Well A08Z

Moreover, the same type of histogram charts were constructed for Pereriv D. Also frequncies of porosity both for Pereriv B and Pereriv D were correlated and the result gave a very high number of correlation coefficent. This can also be concuded as that there is a realitonship of Pereriv B and Pereriv D. Also It was obtained that the mean value of porosity in Pereriv B for A08Z well is 14 and standard deviation os 4.7.

Prencipal Component Analysis also perforemd to get a better understanding of the relationship between porosities of two reservoir formation. The results of th PCA have been also stated in previous chapter. The results of PCA separated two components and based on this two components scatter plots were constructer. Figure 22 is a scatter plots of PCA results of Pereriv B and Pereriv D.

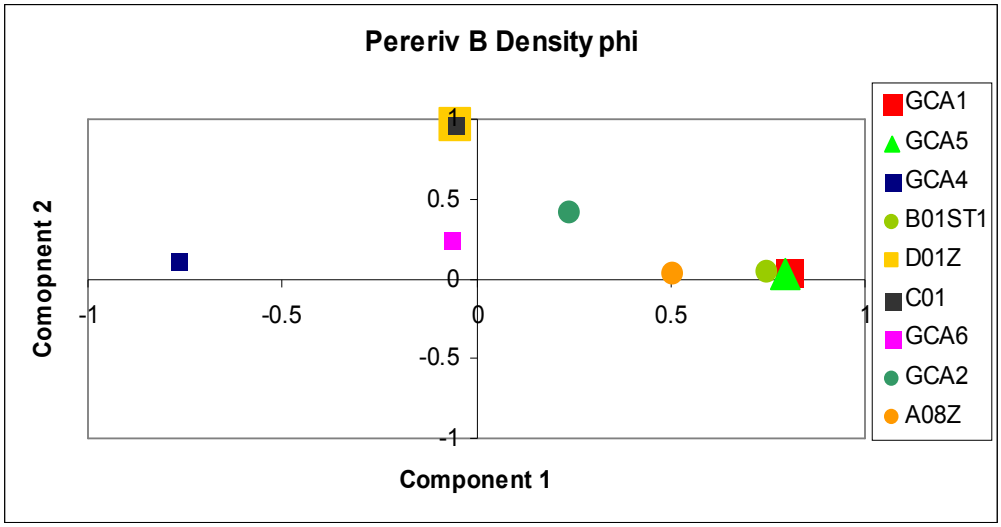


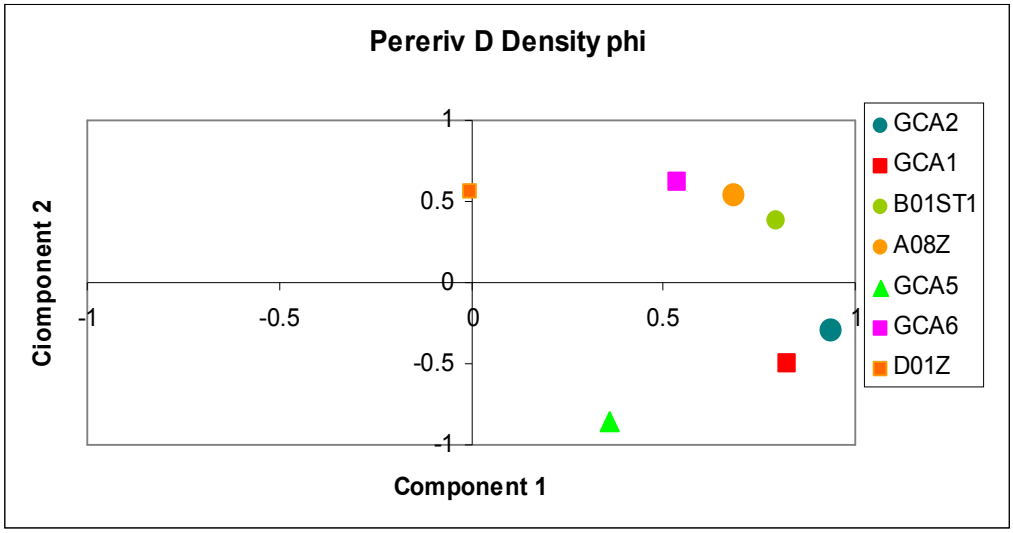


**Figure 23.**Scatter plots of PCA results

Interpretation of the scatter plots showed that porosity is controlled by two factors which could not be identified during our study. In Pereriv B, scatter plots of PCA results indicates that there is no negative effect of second component. Moreover, because of the effect of first component several cluster groups can be distinguished. Also there is a well GCA4 which is completely different from other groups. The reason that can explain this abnormality is that in this well Pereriv B is extremely thick (86 meters) but the thickness for PCA which has been selected is only 11 meters. On the other hand, in Pereriv D PCA result showed no negative effect of first component but both negative and positive influence of second component can be seen. Here is also second cluster groups can be observed.

# CHAPTER 7

# CONCLUSIONS AND RECOMMENDATIONS

1. Volume of shale was calculated from GR and it was obtained than NTG ratio is high in Pereriv D. It contains clean sandstone and average thickness of the Pereriv D is about 25. However, Pereriv B has a slightly higher NTG ratio than Pereriv D. Also Average thickness of the Pereriv B observed in available wells is about 65 meters.
2. One of the crucial points in the reservoir characterization from well loggings was porosity estimation. Mainly, sonic and density logs have been utilized. In some wells sonic log porosity was comparatively higher than density porosity however, for identified flow unit section sonic porosity and density porosities are very identical and correlation coefficient between them was high enough.
3. Based on the core data, especially pores throat size ( $R_{35}$ ) porosity and permeability flow unit determination was performed. Identified flow unit in Pereriv B shows high values of porosity and permeability, and $R_{35}$ . Based on this interpretation upper part of the Pereriv B identified as a flow unit. And these identified flow zone are correlated in all available wells. For defined flow unit, porosity values estimated from density loggings show the same pattern. Therefore, porosity values can give some information of the flow units in other formations.
4. Determined flow zone is pure sandstone zone and can also be characterized by very low Vshale value.
5. Geostatistical method applied to compare Pereriv B and Pereriv D. Histogram have been applied to see the porosity distribution by making frequency plots. Histogram charts of porosity for both Pereriv B and Pereriv D are identical and close to normal distribution. Some of them can be considered as negatively or positively skewed.
6. For both formations, porosity frequency table were constructed. Frequencies of porosity parameter in each well both for Pereriv B and Pereriv D were compared and correlation coefficients were calculated. The results were very high correlation coefficient meaning that they can be related to each other.
7. Principal Component Analysis is another geostatistical method which has also been applied to see how Pereriv B and Pereriv D related to each other. Both Pereriv B and Pereriv D porosity values have been used for PCA testing. In Pereriv B, PCA result gave three components for porosity and two components in Pereriv D.
8. Moreover, scatter plots for determined components showed that in Pereriv B three different cluster groups. On the other hand, two cluster groups can be observed in Pereriv D. Generally with some exceptions these cluster groups show same Vshale, depth and porosity values. Therefore, cluster groups may be interpreted based on above mentioned parameters.

As a recommendation for further work, continuation of the core sampling needs to be performed for Pereriv D. These can lead us better understanding of the reservoir and reliable flow unit determination. Moreover, determination of the flow unit and correlation of them can result in successful reservoir management in the future.

Furthermore, for future works, other statistical methods can also be applied to look for the relationship of two formations. Especially cross correlation can lead to some result in this work.

# REFERENCES


Abbaszadeh, M., Fujii, H., Fujimoto, F., " Permeability Prediction by Hydraulic Flow Units- Theory and Applications " , paper SPE 30158 prepared for presentation at the SPE Petrovietnam Conference held in Hochiminh, Vietnam, 1-3 March, 1995.

Al-Ajmi, F., Holditch, S.A., " Permeability Estimation Using Hydraulic Flow Units in a Central Arabia Reservoir ", paper SPE 63254 prepared for presentation at the 2000 SPE Annual Technical Conference and Exhibition held in Dallas, Texas, 1-4 October, 2000.

Abramovich, M. B., and Sh. F. Mekhtiev 1954, Geology of Azerbaijan oil and gas fields (in Russian): Baku, Elm, 236 p.

Abreu, V., and D. Nummedal, 2007, Miocene to Quaternary sequence stratigraphy of the South and Central Caspian basins, in P. O. Yilmaz and G. H. Isaksen, editors, Oil and gas of the Greater Caspian area: AAPG Studies in Geology 55, p. 65– 86.

Abreu, V.S., Nummedal, D., Ware, P., Self, D., Witmer, R.J., Trevena, A., Williams, E., Trybek, J., (2000). Pliocene/Quaternary sequence stratigraphy of the Caspian Sea region: interplay of deltaic and climatic control on non-marine depositional sequences: Abstract, 1st AAPG Regional International Conference, Istanbul, Turkey.

Aguilera, R., Aguilera, M.S., " The Integration of Capillary Pressures and Pickett Plots for Determination of Flow Units and Reservoir Containers ", paper SPE 71725 prepared for presentation at the 2001 SPE Annual and Technical Conference and Exhibition held in New Orleans, Lousiana, 30 September- 3 October, 2001.

Amaefule, J.O., Altunbay M., Taib, D., Kersey, D.G., Keelan, D.K., "Enhanced Reservoir Description: Using Core and Log Data to Identify Hydraulic (Flow) Units and Predict Permeability in Uncored Intervals/Wells ", paper SPE 26436 prepared for presentation at the 68th Annual Technical Conference and Exhibiton of SPE held in Houston, Texas, 3-6 October, 1993.

Amyx, J., Bass, D., Whiting, R., " Petroleum Reservoir Engineering ", McGraw - Hill Book Company, 610 p., 1960.

Archie, G.E., " The Electrical Resisitivity Log as an Aid in Determining Some Reservoir Characteristics ", Trans. AIME, v.146, p. 54-67,1942.

Azizbekov, Sh. A., 1972, Geology of the USSR, v XLVII: Azerbaijan SSR (in Russian): Moscow, Nedra, 433 p.

Bassiouni, Z., " Theory, Measurement, and Interpretation of Well Logs ", Society of Petroleum Engineers, Richardson, Texas, 372 p., 1994.

Binyatov, E. "Sedimentological, Cyclostratigraphic Analysis and Reservoir Characterization of Balakhany X Formation within the Productive Series on C01 well Azeri Field (Offshore Azerbaijan), Middle East Technical University, 2008/

Buryakovsky, L.A., G.V. Chilingar, and F. Aminzadeh, 2001, Petroleum geology of the South Caspian Basin: Gulf Professional Publishing, 464 p.

Dercourt, J., Zonenshain, L. Ricou, L. Kazmin, V. Le Pichon, X. Knipper, A. Grandjacquet, C. Sbortshikov, I. Geyssant, J. Lepvrier, C. Pechersky, D. Boulin, J. Sibuet, J. Savostin, L. Sorokhtin, O. Westphal, M. Bazhenov, M. Lauer, J. and B. Biju-Duval, 1986, Geologic evolution of the Tethys belt from the Atlantic to the Pamirs since the Lias, in Aubouin, L. Le Pichon, and A. Monin, eds., Evolution of the Tethys: Tectonophysics, vol. 123, nos. 1–4, p. 241–315.

Devlin, W., J. Congswell, G. Gaskins, G. Isaksen, D.P. Pitcher, D. Puls, K. Stanly, and G. Wall, 1999, South Caspian Basin: Young, cool, and full of promise: GSA Today, 9, No.7, p. 1-9.

.

Dumont, H. J., 1998, The Caspian Lake: history, biota, structure, and function: Limnology and Oceanography Vol. 43, p. 44–52.

Ebanks, W.J., Scheihing, M.H., Atkinson, C.D., " Flow Units for Reservoir Characterization ", AAPG Bulletin, p. 282-289, 1984.

Falcon, N., 1974, Southern Iran: Zagros Mountains, in Mesozoic-Cenozoic Orogenic belts: Data for Orogenic Studies, edited by A. Spencer: Geological Society Special Publication, 4, p. 199-211.

Francesco B., Calvin C., Piero C., Giovanni P. R., "Improved Characterization of a Complex Structure In the Azerbaijan Offshore Revealed By 3D Pre-Stack Depth Migration And Depth Continuity Cube Applications", 2001 SEG Annual Meeting, September 9 - 14, 2001 , San Antonio, Texas.

Gunter, G.W., Finneran, J.M., Hartmann, D.J., Miller, J.D., " Early Determination of Reservoir Flow Units Using an Integrated Petrophysical Method ", paper SPE 38679 prepared for presentation at the 1997 SPE Annual Technical Conference and Exhibition held in San Antonio, Texas, 5-8 October, 1997.

Hinds, D.J., E. Aliyeva, M.B. Allen, C.E. Davies, S.B. Kroonenberg, M.D. Simmons, S.J. Vincent, 2004. Sedimentation in a discharge dominated fluviallacustrine system: the Neogene Productive Series of the South Caspian Basin, Azerbaijan: Marine and Petroleum Geology 21, 2004, p. 613-638.

Jones, R.W., and M.D. Simmons, 1997, A review of the stratigraphy of eastern Paratethys (Oligocene-Holocene), with particular emphasis on the Black Sea, in Regional and Petroleum Geology of the Black Sea and Surrounding Regions: American Association of Petroleum Geologists Memoir 68, p. 39-52.

Klimentos,T., " Petrophysics and Seismic Wave technology: Applications in Exploration, Formation Evaluation, and Reservoir Characterization ", paper SPE prepared for presentation at the SPE Middle East Oil Show held in Bahrain, 11-14 March, 1995.

Kroonenberg, S.B., Alekseevski, N.I., Aliyeva, E., Allen, M.B., Aybulatov, D.N., Baba-Zadeh, A., Badyukova, E.N., Davies, C.E., Hinds, D.J., Noogendoorn, R.M., Overeem, I., Rusakova, G.V., Suleymanova, S., Svitoch, A.A., Vincent, S.J., 2005, Two deltas, two basins, one river, one sea: The modern Volga Delta as an analogue of the Neogene Productive Series, South Caspian Basin: SEPM Special Publication No83, p231-258.

Lee, S.H., Datta-Gupta, A., " Electrofacies Characterization and Permeability Predictions in Carbonate Reservoirs: Role of Multivariate Analysis and Nonparameric Regression ", paper SPE 56658 prepared for presentation at the 1999 SPE Annual Technical Conference and Exhiibition held in Houston, Texas, 3-6 October, 1999.

Lucia, F.J., Kerans, C., Senger, R.K., " Defining Flow Units in Dolomitized Carbonate-Ramp Reservoirs ", paper SPE 24702 prepared for presentation at the 67th Annual Technical Conference and Exhibition of SPE held in Washington, D.C., 4-7 October, 1992.

Porras, J.C., Barbato, R., Khazen, L., " Reservoir Flow Units: A Comparison Between Three Models in the Santa Barbara and Pirital Fileds, North Monagas Area, Eastern Venezuela Basin ", paper SPE 53671 prepared for presentation at the 1999 SPE Latin American and Caribbean Petroleum Engineering Conference held in Caracas, Venezuela, 21-23 April, 1999.

Nummedal, D., E. Clifton, 2002, The role of Palaeoclimate in unraveling the reservoir architecture of the Productive Series of the South Caspian Basin, Abstract, Petroleum Geology of the South Caspian Basin International Conference, April 2002, The Geological Society of London, Abstracts, p.15.

Ratchkovski, A., Ogbe, D.O., Lawal, A.S., " Application of Geostatistics and Conventional Methods to derive Hydraulic Flow Units for Improved Reservoir Description: A Case Study of Endicott Field, Alaska ", paper SPE 54587 prepared for presentation at the 1999 SPE Western Regional Meeting held in Anchorage, Alaska, 26-27 May, 1999.

Reynolds A. D., "The Geological Use of Pressure Data: Examples from the Development of the Giant ACG Oilfield, Azerbaijan, Abu Dhabi International Petroleum Exhibition and Conference, 5-8 November 2006, Abu Dhabi, UAE.

Reynolds, A.D., M.D. Simmons, M.B.J. Bowman, J. Henton, A.C. Brayshaw, A.A. Ali-Zade, I.S. Giliyev, S.F. Suleymanova, E.Z. Ateava, D.N. Mamedova, and R.O. Koshkarly, 1998, Implications of outcrop geology for reservoirs in the Neogene Productive Series, Apsheron Peninsula, Azerbaijan: American Association of Petroleum Geologists Bulletin, 82 (1), p. 25-49.

Rincones, J.G., Delgado, R., Ohen, H., Enwere, P.,Guerini,A., Marquez, P., " EffectivePetrophysical Fracture Characterization Using the Flow Unit Concept-San Juan Reservoir, Orocual Fieldi Venezuela ", paper SPE prepared for presentation at the 2000 SPE Annual Technical Conference and Exhibition held in Dallas, Texas, 1-4 October, 2000.

Safarov E., 2007, 3-D seismic reservoir characterization of a petroleum prospect area, Apsheron Ridge, South Caspian Basin: MS thesis, Colorado School of Mines.

Salamov, F.A., 2005, Seismic interpretation of reservoir systems and facies architecture: North Apsheron Ridge, Caspian Sea: MS thesis, Colorado School of Mines.

Smith-Rouch, L.S., 2006, Oligocene-Miocene Maykop/Diatom TotalPetroleum System of the South Caspian Basin Province, Azerbaijan, Iran, andTurkmenistan: USGS, Bulletin 2201-I, Reston, Virginia.

Schlumberger Log Interpretation Charts, Schlumberger Educational Services, U.S.A., 1988.

Uskin, N. I., 1916, Stratigraphy and tectonics of the Productive series of the Balakhany-Sabunchi-Ramany oil-producing region (in Russian): Baku, 80 p. Zonenshain, L.P., and X. Le Pichon, 1986, Deep basins of the Black Sea and Caspian Sea as remnants of Mesozoic back-arc basins: Tectonophysics, 123, p. 181-211.

Zonenshain, L.P., and X. Le Pichon, 1986, Deep basins of the Black Sea and Caspian Sea as remnants of Mesozoic back-arc basins: Tectonophysics, 123, p. 181-211.

# APPENDIX A

## CORE DATA

**Table 20** Core data of well GCA1

| Depth (dd, RKB, m) | Total Macroporosity (excl.Fracture) | $K_{air}$ | $r_{35}$ | k/phi | Calculated Microporosity | Hg Porosity (%) | 400 PSI Porosity (%) | 400 PSI Permeability (Kg) |
|---|---|---|---|---|---|---|---|---|
| 2664.32 | 5.22 | 0.00 | 0.10 | 0 | 10.14794 | 13 | 10.14794 | |
| 2671.09 | 4.29 | 11.36 | 1.79 | 2.648019 | 17.02 | 22 | 20.89 | 13.31182 |
| 2682.39 | 0 | 860.08 | 6.37 | | 10.43869 | 27.6 | 27.45869 | 952.6946 |
| 2685.34 | 11.51 | 82.69 | 0.00 | 7.184188 | 16.91805 | 10 | 16.94805 | 101.0737 |
| 2687.33 | 9.1 | 508.10 | 2.98 | 55.83516 | 14.71458 | 19.7 | 21.38458 | 591.0023 |
| 2698.31 | 4.31 | 0.33 | 0.32 | 0.076566 | 5.996789 | 14 | 6.016789 | 1.117098 |
| 2708.31 | 0.5 | 163.84 | 5.87 | 327.68 | 12.43212 | 25.8 | 23.98212 | 201.5168 |
| 2710.43 | 16.54 | 109.90 | 3.25 | 6.644498 | 15.91339 | 22.4 | 21.14339 | 138.7624 |
| 2770.43 | 0 | 236.03 | 5.87 | | 13.50979 | 24.5 | 23.18979 | 290.2805 |
| 2775.33 | 9.51 | 37.10 | 2.53 | 3.901157 | 8.897928 | 21.9 | 20.84793 | 44.84004 |
| 2780.56 | 3.86 | 520.70 | 0.00 | 134.8964 | 7.23356 | 28 | 25.55356 | 646.261 |
| 2785.1 | 7.77 | 919.50 | 27.80 | 118.3398 | 2.765355 | 31.8 | 24.03535 | 1132.938 |
| 2788.35 | 17.01 | 20.38 | 3.85 | 1.198119 | 8.492469 | 16.1 | 23.38247 | 25.03055 |
| 2792.3 | trace | 11.55 | 2.12 | | 8.479962 | 17.4 | 14.58996 | 14.95345 |
| 2798.35 | 5.67 | 487.99 | 18.60 | 86.06526 | 9.456548 | 33.2 | 23.99655 | 608.641 |
| 2803.3 | trace | 121.17 | 4.19 | | 11.46823 | 22 | 21.79823 | 158.1861 |
| 2808.52 | 3.39 | 318.96 | 8.18 | 94.0885 | 5.545684 | 21.4 | 22.21568 | 409.5793 |
| 2819.36 | 11.11 | 184.83 | 5.39 | 16.63636 | 9.769375 | 25.2 | 22.15937 | 15.98642 |
| 2823.31 | 5.22 | 147.30 | 5.39 | 28.21839 | 14.58612 | 26.6 | 24.13612 | 175.8585 |
| 2829.63 | 8.68 | 0 | 8.18 | 0 | nm | 25 | | |
| 2833.61 | 11.51 | 119.37 | 2.3 | 10.37098 | 17.81 | 22.7 | 26.49 | 138.1452 |
| 2838.34 | 16.32 | 0.47 | 0.54 | 0.028799 | 11.63814 | | 15.02814 | 1.31002 |
| 2848.36 | 18.12 | 17.05 | 0.42 | 0.940949 | 10.91775 | 14.8 | 11.42775 | 20.71136 |
| 2853.1 | 11.49 | 1.41 | 0.7 | 0.122715 | 10.85712 | | 16.07712 | 2.519638 |
| 2854.33 | 4.7 | 0.38 | 1.96 | 0.080851 | 10.46777 | | 15.23777 | 1.115248 |
| 2856.05 | 12.4 | 90.32 | 0.19 | 7.283871 | 11.93579 | | 11.93579 | 117.0754 |
| 2858.27 | 10.32 | 8.43 | 0.91 | 0.81686 | 13.95952 | | 18.27952 | 10.25285 |
| 2866.28 | 14.59 | 0.3 | 0.46 | 0.020562 | 6.772868 | | 7.272868 | 0.938335 |
| 2871.35 | 0.51 | 0 | 0 | 0 | | | | |
| 2882 | 0.96 | | | | | | | |
| 2888 | trace | | | | | | | |
| 2893 | 3.57 | | | | | | | |
| 2896 | 2.77 | | | | | | | |

**Table 21.** Core data of well GCA4

| Depth (dd, RKB, m) | Total Macroporosity (excl.Fracture) | Fracture Macroporosity | Total Macroporosity (incl.Fracture) | Calculated Microporosity | Hg Porosity (%) | Hg Permeability (mD) | 400 PSI Porosity (%) | 400 PSI Permeability (Kg) |
|---|---|---|---|---|---|---|---|---|
| 3125.2 | 19.37 | trace | 19.38 | 6.18 | 27.2 | 520 | 25.55 | 667.793 |
| 3127.5 | 11.9 | trace | 11.91 | 13.59 | 26.6 | 279 | 25.49 | 392.199 |
| 3135.2 | 18.39 | 5.64 | 24.03 | 7.98 | 27 | 1340 | 26.37 | 1977.905 |
| 3138.3 | 8.27 | 0 | 8.27 | 11.12 | 20.8 | 40 | 19.39 | 35.524 |
| 3139.4 | 17.01 | trace | 17.02 | 6.35 | 25.1 | 490 | 23.36 | 707.681 |
| 3143.3 | 13.44 | 0 | 13.44 | 8.45 | 23.4 | 23.6 | 21.89 | 15.689 |
| 3143.6 | 18.15 | 1.21 | 19.36 | 6.89 | 26.1 | 450 | 25.04 | 664.797 |
| 3148.1 | 15.42 | 5.53 | 20.95 | 8.74 | 25.7 | 420 | 24.16 | 558.435 |
| 3155.5 | 16.4 | 1.64 | 18.04 | 10.52 | 27.6 | 670 | 26.92 | 1177.661 |
| 3317.2 | 16.88 | 0.82 | 17.7 | 6.58 | 23.5 | 256 | 23.46 | 571.01 |
| 3319.6 | 11.89 | 0 | 11.89 | 12.81 | 23.9 | 294 | 24.7 | 468.667 |
| 3321.3 | 16.17 | 0.83 | 17 | 7.55 | 25.6 | 500 | 23.72 | 599.439 |
| 3324.5 | 22.79 | 0 | 22.79 | 3.09 | 27 | 760 | 25.88 | 1117.359 |
| 3325.6 | 19.04 | 0 | 19.04 | 3.87 | 26.3 | 580 | 22.91 | 601.994 |

**Table 22.** Core data of well GCA5

| Depth (dd, RKB, m) | Total Macroporosity (excl.Fracture) | Fracture Macroporosity | Total Macroporosity (incl.Fracture) | Calculated Microporosity | Hg Porosity (%) | Hg Permeability (mD) |
|---|---|---|---|---|---|---|
| 2789.1 | 17.88618 | 0.813008 | 18.69919 | 6.740813 | 25.44 | 206.97 |
| 2803.1 | 7.305936 | 1.369863 | 8.675799 | 10.1042 | 18.78 | 14.38 |
| 2805.2 | 15.12605 | 0.840336 | 15.96639 | 10.01361 | 25.98 | 335.91 |
| 2807.1 | 12.93103 | 0.862069 | 13.7931 | 13.9169 | 27.71 | 112.96 |
| 2810.1 | 15 | 1.666667 | 16.66667 | 8.213333 | 24.88 | 95.83 |
| 2860.1 | 8.636364 | 0.454545 | 9.090909 | 13.66909 | 22.76 | 11.48 |
| 2861.1 | 16.94215 | 0.413223 | 17.35537 | 10.02463 | 27.38 | 141.76 |
| 2864.1 | 20.93023 | 1.550388 | 22.48062 | 10.33938 | 32.82 | 726.72 |
| 2879.1 | 17.28395 | 0.411523 | 17.69547 | 11.15453 | 28.85 | 1150.603 |
| 2885.0 | 7.834101 | - | 7.834101 | 12.2959 | 20.13 | 15.75 |
| 2886.2 | 9.41704 | 0.896861 | 10.3139 | 11.3061 | 21.62 | 215.2 |
| 2894.1 | 14.28571 | 1.680672 | 15.96639 | 10.03361 | 26 | 308.09 |
| 2896.1 | 16.87243 | 0.823045 | 17.69547 | 10.02453 | 27.72 | 835.34 |
| 2899.1 | 10.38961 | 3.030303 | 13.41991 | 12.02009 | 25.44 | 236.41 |
| 2902.1 | 13.08017 | 2.531646 | 15.61181 | 9.388186 | 25 | 431.75 |
| 2907.1 | 14.46281 | 2.892562 | 17.35537 | 5.684628 | 23.04 | 1044.05 |
| 2909.1 | 14.22594 | 2.09205 | 16.31799 | 10.41201 | 26.73 | 511.54 |
| 2911.1 | 15.22634 | 2.469136 | 17.69547 | 9.684527 | 27.38 | 1159.807 |
| 2914.1 | 12.80992 | 4.545455 | 17.35537 | 10.25463 | 27.61 | 845.992 |
| 2922.6 | 35.46326 | 0.638978 | 36.10224 | -9.93224 | 26.17 | 739.81 |
| 2927.1 | 20.39216 | 1.176471 | 21.56863 | -0.39863 | 21.17 | 2083.922 |
| 2927.1 | 16.87243 | 0.823045 | 17.69547 | 10.22453 | 27.92 | 800.97 |
| 2938.1 | 11.35371 | 1.310044 | 12.66376 | 12.67624 | 25.34 | 229.733 |
| 2944.1 | 6.511628 | 0.465116 | 6.976744 | 11.64326 | 18.62 | 21.34 |
| 3113.1 | 15.66265 | 4.016064 | 19.67871 | 10.33735 | 26 | 367.77 |
| 3119.1 | 1.960784 | - | 1.960784 | 12.03922 | 14 | 1.0558 |
| 3124.1 | 3.381643 | trace | 3.391643 | 11.61836 | 15 | 2.9665 |
| 3129.1 | 6.511628 | 0.465116 | 6.976744 | 9.488372 | 16 | 5.4917 |

**Table 23.** Core data of well GCA6

| Depth (dd, RKB, m) | Total Macroporosity (excl.Fracture) | Calculated Microporosity | 400 PSI Porosity (%) | 400 PSI Permeability (Kg) | PORhel | $K_{air}$ | $K_{hg}$ | $r_{35}$ |
|---|---|---|---|---|---|---|---|---|
| 3327.06 | 14.16667 | 4.999237 | 21.6659 | 241.2421 | 0.192913 | 190.5796 | 126 | 4.97 |
| 3328.06 | 14.46281 | 5.375863 | 22.73124 | 424.6584 | 0.201803 | 335.4814 | 266 | 6.97 |
| 3329.06 | 10.86957 | 10.53221 | 23.57569 | 139.6493 | 0.209804 | 110.3235 | 88 | 4.2 |
| 3330.07 | | | | | 0.197358 | 225.15 | 162 | 5.41 |
| 3331.07 | 11.53846 | 7.697218 | 22.22713 | 242.5965 | 0.197358 | 191.654 | 173 | 5.41 |
| 3332.06 | | | | | 0.207137 | 117.1728 | 102 | 0 |
| 3333.07 | | | | | 0.187579 | 102.6289 | 87 | 4.57 |
| 3334.06 | | | | | 0.207137 | 249.9639 | 242 | 6.94 |
| 3335.06 | 13.38912 | 6.28379 | 22.60178 | 107.7096 | 0.200914 | 85.0909 | 34 | 3 |
| 3337.06 | | | | | 0.203581 | 150.0763 | 109 | 4.97 |
| 3338.06 | | | | | 0.234695 | 0 | 390 | 8.93 |
| 3339.06 | | | | | 0.246252 | 0 | 470 | 9.74 |
| 3340.06 | 19.77186 | 4.829121 | 28.78349 | 877.3681 | 0.256031 | 693.1223 | 580 | 10.56 |
| 3343.06 | | | | | 0.185801 | 0 | 145 | 4.57 |
| 3344.06 | 14.52282 | 8.234643 | 25.24709 | 197.1155 | 0.224027 | 155.7248 | 141 | 5.89 |
| 3345.06 | | | | | 0.232917 | 110.4657 | 111 | 4.97 |
| 3346.06 | 13.58025 | 6.543792 | 24.23927 | 233.6278 | 0.215137 | 184.5677 | 166 | 5.89 |
| 3347.06 | | | | | 0.069781 | 13.9593 | 25.4 | 3.55 |
| 3348.06 | | | | | 0.207137 | 0 | 410 | 9.68 |
| 3349.07 | 15.68627 | 3.000372 | 24.569 | 493.5366 | 0.218694 | 389.8966 | 370 | 8.21 |
| 3350.11 | | | | | 0.096427 | 0 | 0.00006 | 0 |
| 3351.06 | 8.40708 | 7.844849 | 19.34927 | 87.05144 | 0.171577 | 68.7695 | 64 | 4.2 |
| 3352.06 | | | | | 0.194691 | 166.927 | 162 | 6.38 |
| 3353.05 | 15.6 | 5.232589 | 25.23259 | 685.7063 | 0.224027 | 541.7109 | 440 | 0 |
| 3354.05 | | | | | 0.220472 | 435.764 | 390 | 8.93 |
| 3355.06 | 16.46586 | 6.22944 | 25.90816 | 349.5226 | 0.23025 | 276.1208 | 360 | 8.21 |
| 3356.06 | | | | | 0.208915 | 0 | 430 | 0 |
| 3357.11 | | | | | 0.212471 | 0 | 550 | 10.56 |
| 3360.06 | 14.28571 | 6.408829 | 22.37522 | 69.12772 | 0.199136 | 54.6127 | 157 | 5.9 |
| 3361.06 | | | | | 0.221361 | 0 | 410 | 8.93 |
| 3362.06 | | | | | 0.217805 | 208.2677 | 190 | 6.39 |
| 3363.07 | | | | | 0.216026 | 236.8104 | 205 | 6.95 |
| 3365.06 | | | | | 0.191135 | 0 | 159 | 6.4 |
| 3366.06 | 6.046512 | 8.94855 | 15.92529 | 31.87838 | 0.127343 | 25.1852 | 49 | 3.55 |

**Table 24.** Core data of well C01

| Depth (dd, RKB, m) | MODAL POROSITY(%) | Primary Interparticle Macroporosity | Secondary Intraparticle Macroporosity | Secondary Oversized Macroporosity | Total Macroporosity (excl.Fracture) | Fracture Macroporosity | Calculated Microporosity | Hg Porosity (%) | Hg Permeability (mD) |
|---|---|---|---|---|---|---|---|---|---|
| 2802.13 | 14.89362 | 12.34043 | 0.425532 | 0 | 12.76596 | 2.12766 | 2800.002 | 28.47208 | |
| 2818.02 | | | | | | | | 26.38 | |
| 2820.15 | | | | | | | | 33.09623 | |
| 2822.05 | | | | | | | | 33.50813 | |
| 2827.08 | 16.31799 | 12.97071 | 0.41841 | 0 | 13.38912 | 2.92887 | 2824.151 | 23.73592 | |
| 2830.1 | 0 | 0 | 0 | 0 | | 0 | 2830.1 | 4.766847 | 0.079919 |
| 2836.02 | | | | | | | | 30.13644 | |
| 2839.02 | | | | | | | | 27.61562 | |
| 2843.05 | | | | | | | | 24.05839 | 132.0301 |
| 2848.04 | 22.77992 | 19.30502 | 0 | 0 | 19.30502 | 3.474903 | 2844.565 | 24.84802 | 540.0479 |
| 2859.05 | | | | | | | | 27.81438 | |
| 2860.07 | | | | | | | | 27.00766 | 621.9569 |
| 2864.05 | | | | | | | | 28.04772 | 607.1982 |
| 2879.05 | 23.66412 | 20.61069 | 0.381679 | 0 | 20.99237 | 2.671756 | 2876.378 | 27.62877 | 719.721 |
| 2882.03 | 17.01245 | 14.10788 | 0 | 0 | 14.10788 | 2.904564 | 2879.125 | 23.18765 | 108.2886 |
| 2888.05 | 22.77992 | 18.14672 | 1.930502 | 0 | 20.07722 | 2.702703 | 2885.347 | 25.67053 | 234.3946 |
| 2891.02 | | | | | | | | 24.11953 | |
| 2896.05 | | ) | | | | | | 27.86942 | |

**Table 25. Core data of well D01Z**

| Depth (dd, RKB, m) | MODAL POROSITY(%) | Total Macroporosity (excl.Fracture) | Total Macroporosity (incl.Fracture) | Calculated Microporosity | Hg Porosity (%) | Hg Permeability (mD) |
|---|---|---|---|---|---|---|
| 3714.09 | 25.65056 | 23.79182 | 25.65056 | 3712.231 | 28.04807 | 543.1402 |
| 3716.03 | 25.37313 | 23.13433 | 25.37313 | 3713.791 | 28.96276 | |
| 3718.03 | 13.7931 | 11.63793 | 13.7931 | 3715.875 | 24.30621 | 103.5786 |
| 3719.07 | 23.07692 | 20 | 23.07692 | 3715.993 | 28.19834 | |
| 3720.03 | 23.37165 | 20.30651 | 23.37165 | 3716.965 | 28.76088 | 770.1668 |
| 3722.03 | 19.67871 | 17.26908 | 19.67871 | 3719.62 | 25.57444 | |
| 3725.03 | 22.17899 | 19.45525 | 22.17899 | 3722.306 | 26.56411 | 521.0657 |
| 3727.03 | 21.56863 | 18.03922 | 21.56863 | 3723.501 | 25.42902 | 175.2452 |
| 3728.03 | 22.77992 | 17.76062 | 22.77992 | 3723.011 | 27.79496 | 876.1417 |
| 3731.07 | 24.81203 | 21.05263 | 24.81203 | 3727.311 | 27.39561 | |
| 3736.08 | 22.48062 | 20.54264 | 22.48062 | 3734.142 | 27.97457 | 441.5948 |
| 3740.03 | 28.57143 | 23.57143 | 28.57143 | 3735.03 | 28.87664 | 897.0431 |
| 3742.07 | 26.19926 | 23.61624 | 26.19926 | 3739.487 | 28.41489 | 860.0689 |
| 3745.05 | 18.69919 | 15.85366 | 18.69919 | 3742.204 | 23.66635 | 248.4583 |
| 3746.05 | 22.77992 | 19.69112 | 22.77992 | 3742.961 | 23.71197 | 423.8862 |
| 3747.07 | 26.47059 | 23.52941 | 26.47059 | | 26.7072 | 1038.694 |
| 3749.03 | 20.94862 | 19.36759 | 20.94862 | 3747.449 | 27.4036 | 466.6279 |
| 3752.08 | 19.67871 | 18.07229 | 19.67871 | 3750.474 | 26.27199 | 284.4881 |
| 3754.03 | | | | | 26.25342 | |
| 3756.03 | 30.06993 | 26.92308 | 30.06993 | 0 | 27.71054 | 1047.904 |
| 3759.03 | 20 | 16 | 20 | 3755.03 | 26.52926 | 398.5413 |
| 3762.07 | 26.19926 | 23.24723 | 26.19926 | 3759.118 | 26.62357 | 841.6955 |
| 3763.03 | 18.69919 | 15.44715 | 18.69919 | 3759.778 | 25.31241 | 506.8272 |
| 3766.03 | 27.53623 | 22.10145 | 27.53623 | 0 | 27.31949 | |
| 3769.08 | 24.5283 | 20.75472 | 24.5283 | 3765.306 | 25.11403 | |
| 3771.03 | 22.17899 | 20.23346 | 22.17899 | 3769.084 | 24.87103 | 256.2544 |

## APPENDIX B

## RESULTS OF PCA

**Pereriv B. Density Porosity**

**Table 26** Correlation matrix (Pereriv B)

**Correlation Matrix**

| | | A08Z | B01ST1 | D01Z | GCA1 | GCA2 | GCA4 | GCA5 |
|---|---|---|---|---|---|---|---|---|
| Correlation | A08Z | 1.000 | .082 | .034 | .410 | .132 | -.402 | .171 |
| | B01ST | .082 | 1.000 | -.063 | .603 | .191 | -.343 | .607 |
| | D01Z | .034 | -.063 | 1.000 | -.027 | .201 | .082 | .039 |
| | GCA1 | .410 | .603 | -.027 | 1.000 | .179 | -.417 | .480 |
| | GCA2 | .132 | .191 | .201 | .179 | 1.000 | -.143 | -.003 |
| | GCA4 | -.402 | -.343 | .082 | -.417 | -.143 | 1.000 | -.599 |
| | GCA5 | .171 | .607 | .039 | .480 | -.003 | -.599 | 1.000 |
| | GCA6 | -.250 | .315 | .053 | .094 | .284 | .369 | -.098 |
| | C01 | .034 | -.063 | 1.000 | -.027 | .201 | .082 | .039 |

**Correlation Matrix**

| | | GCA6 | C01 |
|---|---|---|---|
| Correlation | A08Z | -.250 | .034 |
| | B01ST1 | .315 | -.063 |
| | D01Z | .053 | 1.000 |
| | GCA1 | .094 | -.027 |
| | GCA2 | .284 | .201 |
| | GCA4 | .369 | .082 |
| | GCA5 | -.098 | .039 |
| | GCA6 | 1.000 | .053 |
| | C01 | .053 | 1.000 |

**Table 27.** Communalities (Pereriv B)

**Communalities**

| | Initial | Extraction |
|---|---|---|
| A08Z | 1.000 | .744 |
| B01ST1 | 1.000 | .853 |
| D01Z | 1.000 | .996 |
| GCA1 | 1.000 | .682 |
| GCA2 | 1.000 | .734 |
| GCA4 | 1.000 | .740 |
| GCA5 | 1.000 | .840 |
| GCA6 | 1.000 | .839 |
| C01 | 1.000 | .996 |

**Table 28.** Total Variance Explained (Pereriv B)

**Total Variance Explained**

| Component | Initial Eigenvalues | | | Extraction Sums of Squared Loadings | | |
|---|---|---|---|---|---|---|
| | Total | % of Variance | Cumulative % | Total | % of Variance | Cumulative % |
| 1 | 2.744 | 30.486 | 30.486 | 2.744 | 30.486 | 30.486 |
| 2 | 2.108 | 23.422 | 53.908 | 2.108 | 23.422 | 53.908 |
| 3 | 1.557 | 17.304 | 71.212 | 1.557 | 17.304 | 71.212 |
| 4 | 1.016 | 11.291 | 82.503 | 1.016 | 11.291 | 82.503 |
| 5 | .712 | 7.911 | 90.414 | | | |
| 6 | .361 | 4.007 | 94.421 | | | |
| 7 | .268 | 2.982 | 97.403 | | | |
| 8 | .234 | 2.597 | 100.000 | | | |
| 9 | -4.983E-016 | -5.537E-015 | 100.000 | | | |

**Table 29.** Total Variance Explained (Pereriv B)

**Total Variance Explained**

| Component | Rotation Sums of Squared Loadings | | |
|---|---|---|---|
| | Total | % of Variance | Cumulative % |
| 1 | 2.409 | 26.763 | 26.763 |
| 2 | 2.024 | 22.487 | 49.251 |
| 3 | 1.665 | 18.502 | 67.752 |
| 4 | 1.328 | 14.751 | 82.503 |
| 5 | | | |
| 6 | | | |
| 7 | | | |
| 8 | | | |
| 9 | | | |

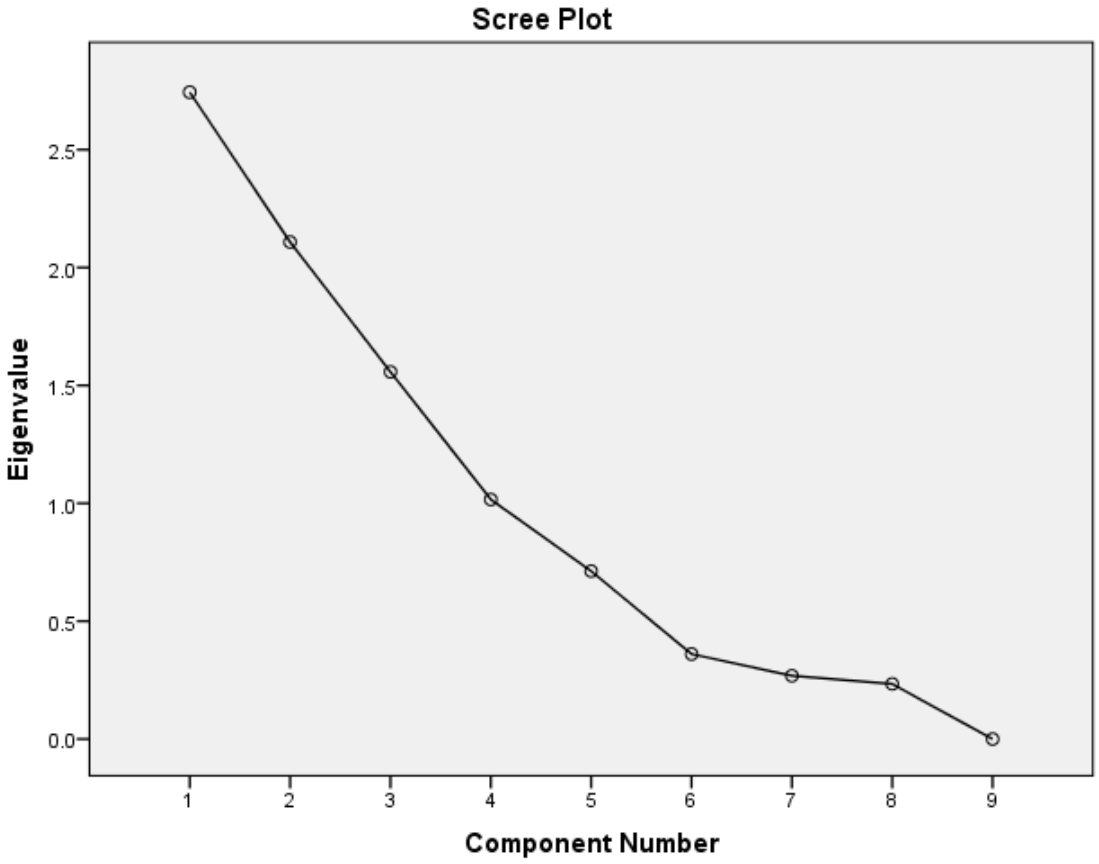


**Figure 24.** Scree plot (Pereriv B)

**Table 30.** Component matrix (Pereriv B)

**Component Matrix**

| | Component | | | |
|---|---|---|---|---|
| | 1 | 2 | 3 | 4 |
| GCA1 | .802 | .043 | .165 | .100 |
| GCA5 | .795 | .029 | -.044 | -.453 |
| GCA4 | -.766 | .113 | .374 | -.018 |
| B01ST1 | .748 | .036 | .489 | -.232 |
| D01Z | -.052 | .965 | -.205 | -.144 |
| C01 | -.052 | .965 | -.205 | -.144 |
| GCA6 | -.065 | .240 | .879 | .066 |
| GCA2 | .241 | .414 | .323 | .633 |
| A08Z | .504 | .035 | -.433 | .548 |

**Table 31.** Reproduced Correlations (Pereriv B)

**Reproduced Correlations**

| | | A08Z | B01ST1 | D01Z | GCA1 | GCA2 | GCA4 |
|---|---|---|---|---|---|---|---|
| Reproduced Correlation | A08Z | .744[a] | .039 | .018 | .390 | .343 | -.555 |
| | B01ST1 | .039 | .853[a] | -.071 | .658 | .207 | -.382 |
| | D01Z | .018 | -.071 | .996[a] | -.048 | .230 | .075 |
| | GCA1 | .390 | .658 | -.048 | .682[a] | .328 | -.550 |
| | GCA2 | .343 | .207 | .230 | .328 | .734[a] | -.029 |
| | GCA4 | -.555 | -.382 | .075 | -.550 | -.029 | .740[a] |
| | GCA5 | .173 | .679 | .061 | .586 | -.097 | -.614 |
| | GCA6 | -.369 | .375 | .045 | .110 | .410 | .404 |
| | C01 | .018 | -.071 | .996 | -.048 | .230 | .075 |
| Residual[b] | A08Z | | .043 | .016 | .021 | -.211 | .153 |
| | B01ST1 | .043 | | .007 | -.055 | -.015 | .038 |
| | D01Z | .016 | .007 | | .021 | -.029 | .007 |
| | GCA1 | .021 | -.055 | .021 | | -.149 | .133 |
| | GCA2 | -.211 | -.015 | -.029 | -.149 | | -.114 |
| | GCA4 | .153 | .038 | .007 | .133 | -.114 | |
| | GCA5 | -.001 | -.072 | -.022 | -.106 | .095 | .015 |
| | GCA6 | .118 | -.061 | .008 | -.016 | -.125 | -.036 |
| | C01 | .016 | .007 | .004 | .021 | -.029 | .007 |

**Table 32.** Reproduced Correlations (Pereriv B)

**Reproduced Correlations**

| | | GCA5 | GCA6 | C01 |
|---|---|---|---|---|
| Reproduced Correlation | A08Z | .173[a] | -.369 | .018 |
| | B01ST1 | .679 | .375[a] | -.071 |
| | D01Z | .061 | .045 | .996[a] |
| | GCA1 | .586 | .110 | -.048 |
| | GCA2 | -.097 | .410 | .230 |
| | GCA4 | -.614 | .404 | .075 |
| | GCA5 | .840 | -.113 | .061 |
| | GCA6 | -.113 | .839 | .045 |
| | C01 | .061 | .045 | .996 |
| Residual[b] | A08Z | -.001 | .118 | .016 |
| | B01ST1 | -.072 | -.061 | .007 |
| | D01Z | -.022 | .008 | .004 |
| | GCA1 | -.106 | -.016 | .021 |
| | GCA2 | .095 | -.125 | -.029 |
| | GCA4 | .015 | -.036 | .007 |
| | GCA5 | | .015 | -.022 |
| | GCA6 | .015 | | .008 |
| | C01 | -.022 | .008 | |

**Table 33.** Rotated component matrix (Pereriv B)

**Rotated Component Matrix**

| | Component | | | |
|---|---|---|---|---|
| | 1 | 2 | 3 | 4 |
| B01ST1 | .877 | -.076 | .176 | .217 |
| GCA5 | .870 | .097 | -.165 | -.218 |
| GCA1 | .715 | -.061 | -.249 | .325 |
| D01Z | -.018 | .994 | .010 | .086 |
| C01 | -.018 | .994 | .010 | .086 |
| A08Z | .126 | .001 | -.793 | .315 |
| GCA6 | .146 | -.007 | .711 | .559 |
| GCA4 | -.575 | .053 | .635 | .067 |
| GCA2 | .061 | .161 | -.091 | .835 |

**Table 34.** Component transformation matrix

**Component Transformation Matrix**

| Component | 1 | 2 | 3 | 4 |
|---|---|---|---|---|
| 1 | .886 | -.048 | -.421 | .187 |
| 2 | .025 | .942 | .089 | .323 |
| 3 | .253 | -.253 | .786 | .504 |
| 4 | -.387 | -.214 | -.444 | .779 |

**Pereriv D Density Porosity**

**Table 35.** Correlation matrix (Pereriv D)

**Correlation Matrix**

| | | A08Z | B01ST1 | D01Z | GCA1 | GCA2 | GCA5 | GCA6 |
|---|---|---|---|---|---|---|---|---|
| Correlation | A08Z | 1.000 | .753 | .135 | .243 | .476 | -.259 | .497 |
| | B01ST1 | .753 | 1.000 | .171 | .379 | .582 | .005 | .519 |
| | D01Z | .135 | .171 | 1.000 | -.181 | -.169 | -.235 | .294 |
| | GCA1 | .243 | .379 | -.181 | 1.000 | .930 | .718 | .199 |
| | GCA2 | .476 | .582 | -.169 | .930 | 1.000 | .560 | .352 |
| | GCA5 | -.259 | .005 | -.235 | .718 | .560 | 1.000 | -.360 |
| | GCA6 | .497 | .519 | .294 | .199 | .352 | -.360 | 1.000 |
| Sig. (1-tailed) | A08Z | | .000 | .216 | .077 | .002 | .063 | .001 |
| | B01ST1 | .000 | | .159 | .011 | .000 | .488 | .001 |
| | D01Z | .216 | .159 | | .146 | .162 | .083 | .041 |
| | GCA1 | .077 | .011 | .146 | | .000 | .000 | .122 |
| | GCA2 | .002 | .000 | .162 | .000 | | .000 | .018 |
| | GCA5 | .063 | .488 | .083 | .000 | .000 | | .015 |
| | GCA6 | .001 | .001 | .041 | .122 | .018 | .015 | |

**Table 36.** KMO and Bartlett's Test (Pereriv D)

**KMO and Bartlett's Test**

| | | |
|---|---|---|
| Kaiser-Meyer-Olkin Measure of Sampling Adequacy. | | .573 |
| Bartlett's Test of Sphericity | Approx. Chi-Square | 205.189 |
| | df | 21 |
| | Sig. | .000 |

**Table 37.** Anti-image matrices (Pereriv D)

**Anti-image Matrices**

| | | A08Z | B01ST1 | D01Z | GCA1 | GCA2 | GCA5 |
|---|---|---|---|---|---|---|---|
| Anti-image Covariance | A08Z | .222 | -.128 | -.078 | .008 | -.047 | .105 |
| | B01ST1 | -.128 | .301 | -.070 | .042 | -.032 | -.052 |
| | D01Z | -.078 | -.070 | .710 | -.026 | .069 | -.072 |
| | GCA1 | .008 | .042 | -.026 | .065 | -.045 | -.034 |
| | GCA2 | -.047 | -.032 | .069 | -.045 | .051 | -.019 |
| | GCA5 | .105 | -.052 | -.072 | -.034 | -.019 | .134 |
| | GCA6 | .100 | -.076 | -.175 | -.019 | -.040 | .144 |
| Anti-image Correlation | A08Z | .542[a] | -.494 | -.197 | .069 | -.442 | .607 |
| | B01ST1 | -.494 | .708[a] | -.151 | .303 | -.259 | -.259 |
| | D01Z | -.197 | -.151 | .383[a] | -.120 | .361 | -.232 |
| | GCA1 | .069 | .303 | -.120 | .657[a] | -.775 | -.365 |
| | GCA2 | -.442 | -.259 | .361 | -.775 | .622[a] | -.235 |
| | GCA5 | .607 | -.259 | -.232 | -.365 | -.235 | .474[a] |
| | GCA6 | .389 | -.253 | -.379 | -.140 | -.324 | .722 |

**Anti-image Matrices**

| | | GCA6 |
|---|---|---|
| Anti-image Covariance | A08Z | .100 |
| | B01ST1 | -.076 |
| | D01Z | -.175 |
| | GCA1 | -.019 |
| | GCA2 | -.040 |
| | GCA5 | .144 |
| | GCA6 | .298 |
| Anti-image Correlation | A08Z | .389[a] |
| | B01ST1 | -.253 |
| | D01Z | -.379 |
| | GCA1 | -.140 |
| | GCA2 | -.324 |
| | GCA5 | .722 |
| | GCA6 | .472 |

**Table 38.** Communalities (Pereriv D)

**Communalities**

| | Initial | Extraction |
|---|---|---|
| A08Z | 1.000 | .749 |
| B01ST1 | 1.000 | .778 |
| D01Z | 1.000 | .310 |
| GCA1 | 1.000 | .926 |
| GCA2 | 1.000 | .965 |
| GCA5 | 1.000 | .861 |
| GCA6 | 1.000 | .669 |

**Table 39.** Total variance explained (Pereriv D)

**Total variance explained**

| Component | Initial Eigenvalues | | | Extraction Sums of Squared Loadings | | |
|---|---|---|---|---|---|---|
| | Total | % of Variance | Cumulative % | Total | % of Variance | Cumulative % |
| 1 | 3.075 | 43.926 | 43.926 | 3.075 | 43.926 | 43.926 |
| 2 | 2.184 | 31.198 | 75.124 | 2.184 | 31.198 | 75.124 |
| 3 | .846 | 12.081 | 87.206 | | | |
| 4 | .553 | 7.895 | 95.100 | | | |
| 5 | .246 | 3.511 | 98.612 | | | |
| 6 | .066 | .943 | 99.555 | | | |
| 7 | .031 | .445 | 100.000 | | | |

**Table 40.** Total variance explained (Pereriv D)

**Total variance explained**

| Component | Rotation Sums of Squared Loadings | | |
|---|---|---|---|
| | Total | % of Variance | Cumulative % |
| 1 | 2.697 | 38.531 | 38.531 |
| 2 | 2.562 | 36.593 | 75.124 |
| 3 | | | |
| 4 | | | |
| 5 | | | |
| 6 | | | |
| 7 | | | |

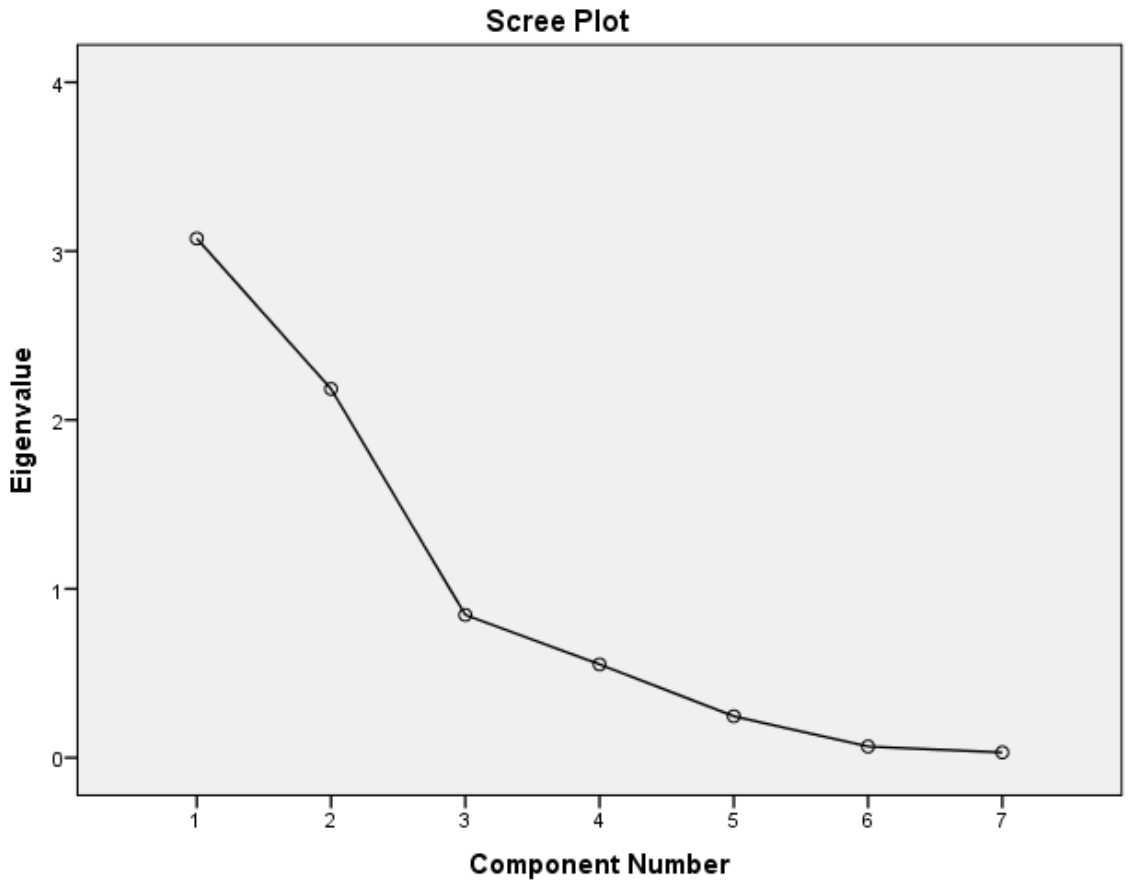


**Figure 25.** Scree plot (Pereriv D)

**Table 41.** Component matrix (Pereriv D)

**Component matrix**

| | Component | |
|---|---|---|
| | 1 | 2 |
| GCA2 | .937 | -.294 |
| GCA1 | .822 | -.500 |
| B01ST1 | .796 | .380 |
| A08Z | .684 | .530 |
| GCA5 | .360 | -.855 |
| GCA6 | .538 | .616 |
| D01Z | -.002 | .557 |

**Table 42.** Reproduced correlations (Pereriv D)

**Reproduced correlations**

| | | A08Z | B01ST1 | D01Z | GCA1 | GCA2 | GCA5 |
|---|---|---|---|---|---|---|---|
| Reproduced Correlation | A08Z | .749[a] | .746 | .294 | .297 | .485 | -.207 |
| | B01ST1 | .746 | .778[a] | .210 | .465 | .634 | -.038 |
| | D01Z | .294 | .210 | .310[a] | -.281 | -.166 | -.477 |
| | GCA1 | .297 | .465 | -.281 | .926[a] | .918 | .724 |
| | GCA2 | .485 | .634 | -.166 | .918 | .965[a] | .589 |
| | GCA5 | -.207 | -.038 | -.477 | .724 | .589 | .861[a] |
| | GCA6 | .695 | .662 | .342 | .134 | .323 | -.333 |
| Residual[b] | A08Z | | .007 | -.159 | -.054 | -.009 | -.052 |
| | B01ST1 | .007 | | -.038 | -.085 | -.053 | .043 |
| | D01Z | -.159 | -.038 | | .100 | -.003 | .242 |
| | GCA1 | -.054 | -.085 | .100 | | .012 | -.007 |
| | GCA2 | -.009 | -.053 | -.003 | .012 | | -.030 |
| | GCA5 | -.052 | .043 | .242 | -.007 | -.030 | |
| | GCA6 | -.197 | -.143 | -.048 | .065 | .029 | -.027 |

**Table 43.** Reproduced correlations (Pereriv D)

**Reproduced correlations**

| | | GCA6 |
|---|---|---|
| Reproduced Correlation | A08Z | .695[a] |
| | B01ST1 | .662 |
| | D01Z | .342 |
| | GCA1 | .134 |
| | GCA2 | .323 |
| | GCA5 | -.333 |
| | GCA6 | .669 |
| Residual[b] | A08Z | -.197 |
| | B01ST1 | -.143 |
| | D01Z | -.048 |
| | GCA1 | .065 |
| | GCA2 | .029 |
| | GCA5 | -.027 |
| | GCA6 | |

**Table 44.** Rotated Component Matrix (Pereriv D)

**Rotated Component Matrix**

| | Component | |
|---|---|---|
| | 1 | 2 |
| A08Z | .864 | .043 |
| B01ST1 | .851 | .230 |
| GCA6 | .810 | -.118 |
| GCA1 | .298 | .915 |
| GCA5 | -.283 | .884 |
| GCA2 | .520 | .833 |
| D01Z | .361 | -.424 |

**Table 45.** Component transformation matrix (Pereriv D)

**Component transformation matrix**

| Component | 1 | 2 |
|---|---|---|
| 1 | .759 | .651 |
| 2 | .651 | -.759 |